ELASTIC AND INELASTIC COLLISIONS OF NUCLEONS AT HIGH ENERGIES

K. D. Tolstov

Experimental data obtained in proton-proton and proton-neutron collisions at high energy are reviewed, including elastic scatterings, generation of particles and resonances, and momentum spectra of secondary particles. The results of experiments are compared with the theoretical models.

INTRODUCTION

In formulating a theory of strong interaction the investigation of elastic and inelastic collisions between nucleons occupies a central position. From the experimental point of view we are dealing with the most intense primary proton beams which exceed the intensity of secondary particles by many orders, and by using hydrogen targets we can investigate interactions between identical particles. This has allowed, for example, the achievement of differential cross sections $\sim 10^{-36}$ cm^2 for elastic pp-scattering.

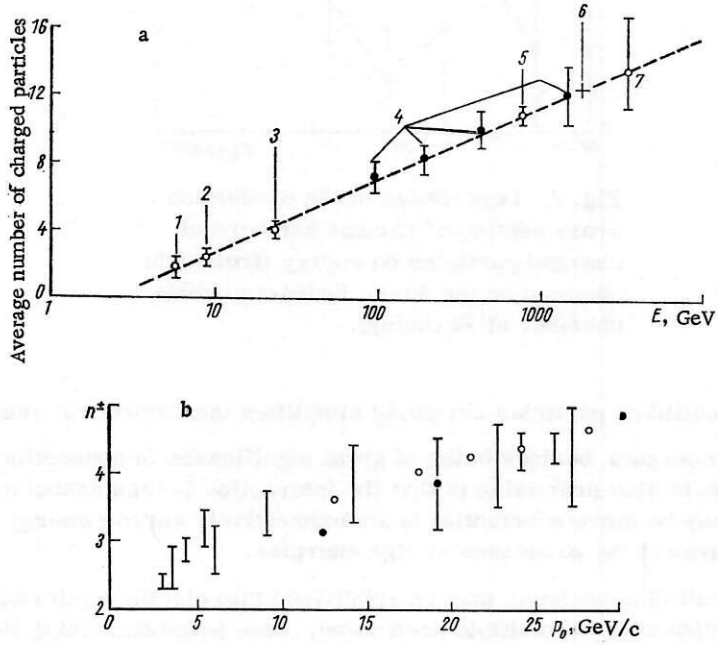

Fig. 1. Dependence of the average number of charged particles on photon energy (a) according to the data obtained at: 1) Berkeley; 2) Dubna; 3) CERN; 4) Physics Institute of the Academy of Sciences of the USSR (Moscow); 5) Tokyo (photoemulsion data); 6) predictions for the CERN colliding-beam accelerator; 7) Chicago (photoemulsion data). The experimental and calculated values of the average number of charged particles in pp-collisions as a function of energy (b): ○) are the experimental data; ●) are the calculated results.

Joint Institute for Nuclear Research, Dubna. Translated from Problemy Fiziki Elementarnykh Chastits i Atomnogo Yadra, Vol. 2, No. 1, pp. 231–278, 1971.

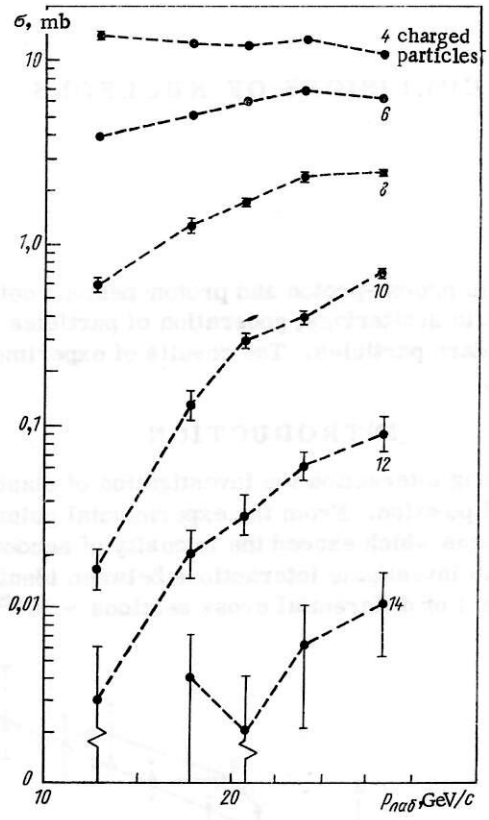

Fig. 2. Dependence of the production cross section of various numbers of charged particles on energy (from data obtained on the 80-in. hydrogen bubble chamber at Berkeley).

The identity of the colliding particles obviously simplifies the theoretical analysis.

The ranges of high energies, besides being of great significance in connection with the asymptotic behavior of the processes, is also promising in that the interaction is less associated with resonance phenomena. The latter may be more substantial in a comparatively narrow energy range and thus may not reflect the basic features of the processes at high energies.

The interaction of colliding nucleons may be subdivided into elastic scattering, scattering with charge exchange, quasiparticle reactions, and multiple production, these processes being linked by relationships which derive from the unitarity properties of the S-matrix.

For specific colliding particles the S-matrix depends on the energy and angular momentum, and its unitarity also relates the elastic scattering to all of the remaining processes for a fixed value of angular momentum. If data were to be available on the dependence of the interactions on the angular momentum (i.e., on the impact parameter), then it would be possible to obtain many important conclusions, including conclusions concerning the so-called central and peripheral collisions (which for the time being have an arbitrary character) and consequently concerning the structural features of nucleons in strong interactions.

I. INELASTIC pp-COLLISIONS

1.1. The Multiplicity of the Particles

The dependence of the number of charged particles in pp-collisions on energy n(E) in the laboratory system is displayed in Fig. 1. From Fig. 1a it follows that in the 100 to 1000 GeV range where there are more points and the error is smaller, we have $n(E) \sim aE^{1/3}$.

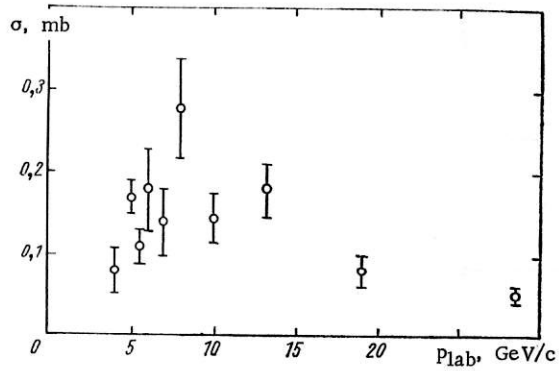

Fig. 3. The dependence of the total ω-meson production cross section in pp collisions on proton momentum.

In accordance with Fig. 1b we have $n(E) \sim aE^{0.4}$ in the 10 to 30 Ge V range. Thus, the growth of n(E) occurs substantially faster than the $E^{1/4}$ which was obtained in the Fermi statistical theory and the Landau hydrodynamic theory, or than the logarithmic growth $n(E) \sim \log(E)$ obtained according to the multiperipheral model.

In this connection one should dwell on the recent paper by P. Rotelly [1] in which the author does not use the model involving the formation of one or several fireballs in considering statistically multiple production of particles. Rotelly notes that previously no statistical consideration of multiple production had been carried out which was not based on the concept of the merging of colliding particles. In reality a process without merging is more natural, since we do not have an equilibrium state during collision but more likely an explosion.

Rotelly bases himself on the classical graincanonical distributions, postulating that the entropy does not depend on energy in the center of mass system for a fairly high energy of the primary particles. Further he starts from a constant inelasticity coefficient which is equal to 0.4 in the center of mass system (i.e., the secondary particles carry away on the average a constant energy fraction equal to $-0.4E_c$). This leads to the following formulas for the number of generated π- and K-mesons:

$$n_\pi = 4(E_\pi/m_\pi)^{2/3}; \quad (1)$$

$$n_K = 4(E_K/m_K), \quad (2)$$

where E_π, E_K are the energies of π- and K-mesons in the center of mass system, while m_π, m_K are their masses. Consequently the dependence of the number of particles on energy in the laboratory coordinate system can be expressed by the law $E^{1/3}$.

In explaining multiple production R. Hagedorn [2] starts from the fact that thermodynamic equilibrium and collective motion along the collision axis holds in collisions at high energies. The simplest method of separating these processes is to consider quantities which do not depend on the collective motion – the multiplicity of the particles is among them.

According to Hagedorn, the multiplicity follows the law ~exp (–m/T), where the temperature $T \to T_0$, T_0 increasing with energy so that $T_0 \sim 160$ MeV at high energies. The results of the calculations carried out by Hagedorn and Ranft are plotted in Fig. 1b (the filled circles). Let us note that according to Hagedorn the onset of saturation of the number of produced particles must occur at high energies, which does not derive from the data shown in Fig. 1a. The energy dependence of the production cross sections of various numbers of charged particles is shown in Fig. 2.

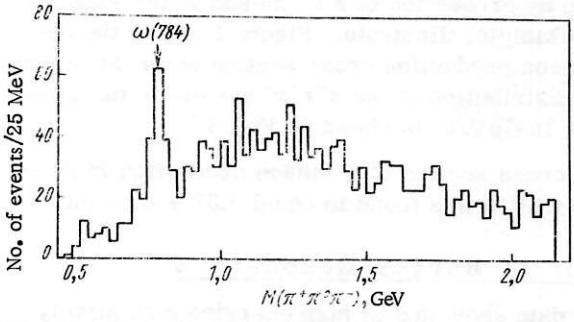

Fig. 4. Distribution of the effective masses of the $\pi^+\pi^-\pi^0$ system in the $pp \to pp\pi^+\pi^-\pi^0$ reaction at 19 GeV/c.

1.2. Production of Strange Particles

Calculations of the production of strange particles have usually led to a small fraction of them as compared with π-mesons. However, Rotelly in [1], using Eqs. (1) and (2) and assuming that at high energies the equation $E_\pi = E_K = 1/3E_c$ holds asymptotically, obtained $N_K/N_\pi = 0.43$. Such a high fraction of K-mesons is a new result which may serve as a check of the Rotelly concept.

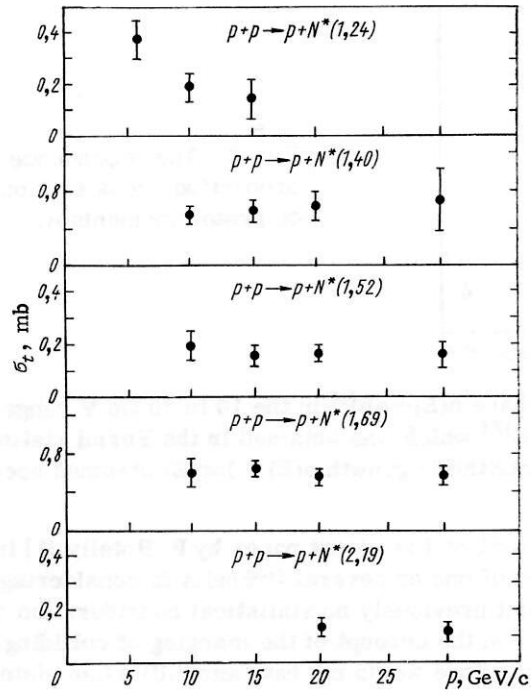

Fig. 5. Dependence of the total cross section of isobar production in the $pp \rightarrow p + N^*$ reaction on proton momentum.

The experimental data on the total cross sections of the production of strange particles in pp-collisions are as yet not numerous. At 8 GeV Firebugh et al. [3] obtained $\sigma_{tot} = 1.8$ mb; Holmgren et al. [4] obtained $\sigma_{tot} = 2.05 \pm 0.14$ mb at 10 GeV, assuming equality of the production cross sections of YK^+ and YK^0; Bartke et al. [5] obtained the production cross section YK 3.0 ± 0.3 mb for the production of YK and and a cross section KK 1.2 ± 0.3 mb for a pair production of KK at 24.5 GeV (i.e., $\sigma_{tot} = 4.2 \pm 0.4$ mb, which is ~ 0.15 of the total inelastic cross section). Consequently, a substantial growth of the cross section with increasing photon energy is observed.

At cosmic energies the ratio between the number of K-mesons and the number of π-mesons is estimated to be 0.2 to 0.4. Thus, the experimental data do not contradict the Rotelly calculations. (Let us note likewise that in πp-collisions at 25 GeV the production cross section of K-mesons is $\geqslant 4$ mb according to the data cited by Erwin [6]; i.e., it is more than 0.2 of the inelastic cross section.)

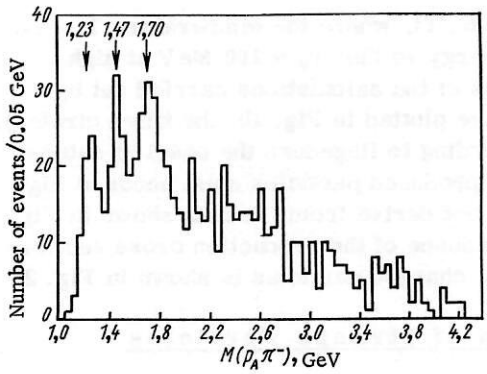

Fig. 6. Effective mass distribution of the $p\pi^-$ system in the case when a Δ^{++} isobar is formed in the $pp \rightarrow pp\pi^+\pi^-$ reaction at 16 GeV/c.

1.3. Production of Boson Resonance

Boson resonances yield a relatively small contribution to the total cross section in pp-collisions at high energies, especially in events having a large multiplicity of particles. The largest contribution is made by production of a ω^0 meson which Figs. 3 and 4 from [7], for example, illustrate. Figure 3 shows the dependence of the ω-meson production cross section on proton energy. The effective mass distribution of the $\pi^+\pi^-\pi^0$ system in the $pp \rightarrow pp\pi^+\pi^-\pi^0$ reaction at 19 GeV/c is shown in Fig. 4.

The resultant cross section of ρ-meson production in $pp \rightarrow \Delta\rho N$ reactions at 19 GeV/c was found to equal 0.57 ± 0.07 mb.

1.4. Production of Baryon Resonances

Experimental data show that at high energies a relatively small fraction of baryon resonances is formed, similarly to boson

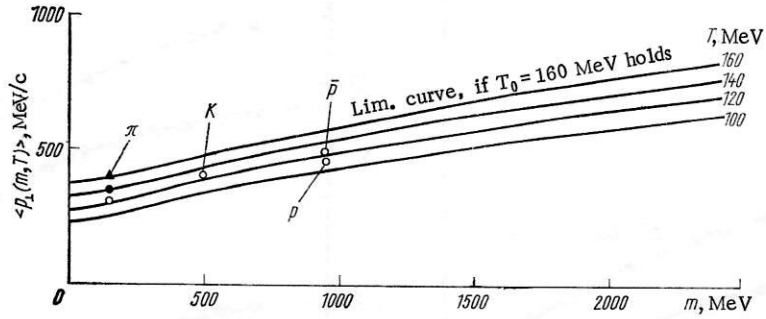

Fig. 7. Dependence of the average transverse momentum of the secondary particles on their mass and on the temperature of the excited system: ○) is for 12 to 30 GeV/c (different experiments); Δ) is for 10^3 to 10^5 GeV/c (Kranov); ●) is for $3 \cdot 10^3$ GeV/c (Brazilian-Japanese collaboration).

resonances. Consequently, it is also true that the possible cascade decay of baryon resonances will not make a significant contribution to the multiple production of particles.

Figure 5 shows the dependence of the total cross section of the production of baryon resonances having different masses on the proton momentum according to the data published by Anderson et al. [8]. At 30 GeV/c the sum of the total cross sections is $\Sigma\sigma_{tot}(M) = 1.7 \pm 0.4$ mb. In reactions with production of two mesons, as Bertocchi notes [9], the probability of the transition of both colliding protons into a resonance state is low, since the charge conservation prevents the formation of two Δ^{++} isobars and the isotopic spin relationships reduce the probability of the formation of the Δ^0 isobar. However, in the paper by Rushbrooke [10] there is an indication of double production of Δ^{++}, Δ^0 isobars. This is evident from Fig. 6, where the dependence of the number of events on the mass of the $p\pi^-$ system is given in cases when Δ^{++} isobars are formed.

1.5. The Momentum Spectra

At present the general regularities governing the momentum spectra and the emission-angle distribution of secondary protons and particles produced in inelastic collisions are well known. A strong collimation of protons in the center of mass system is observed in the direction of the primary momentum.

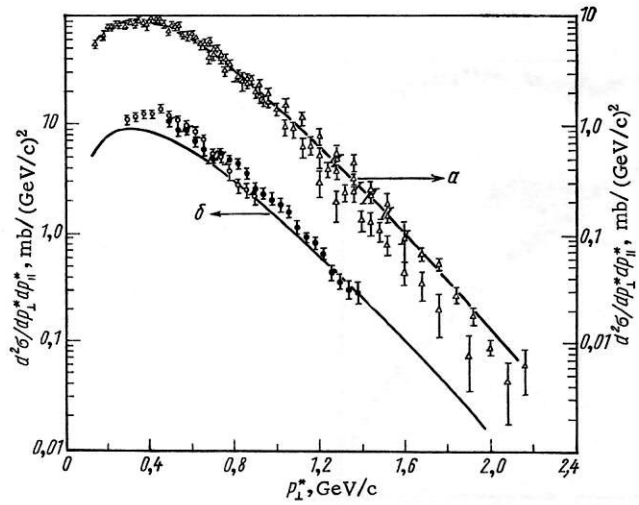

Fig. 8. Spectrum of secondary protons as a function of $p_\perp$ in pp collisions at momenta of 10, 20, 30 GeV/c: a) $p_0 = 30$ GeV/c; b) ○ is for $p_0 = 10$ GeV/c; ● is for $p_0 = 20$ GeV/c; the solid line is for the fictitious curve at 30 GeV/c.

The average inelasticity coefficient k and the average transverse momentum of protons are practically constant over a wide energy range and are equal to $\langle k \rangle \simeq 0.4 - 0.5$; $\langle p\perp \rangle \sim 0.4$ Ge V/c. Predominant emission of $\pi\pm$ and K± mesons in the direction of primary protons and a more pronounced emission for positive particles are observed in the center of mass system. With increasing multiplicity of the secondary particles this directivity decreases.

The momentum spectra and the dependence of the cross sections on the momenta are very essential for clarifying the mechanism of inelastic collisions. Hagedorn, for example, assumed that the distribution over the primary momenta $N(p\perp)$ of the produced particles does not depend on their collective motion along the collision axis and follows a Boltzmannian distribution (i.e., $N(p\perp) \sim \exp(-(p\perp)/(T))$. This dependence is analogous to the previously considered distribution for multiple production of particles according to the Hagedorn scheme. At 30 GeV the tempera-

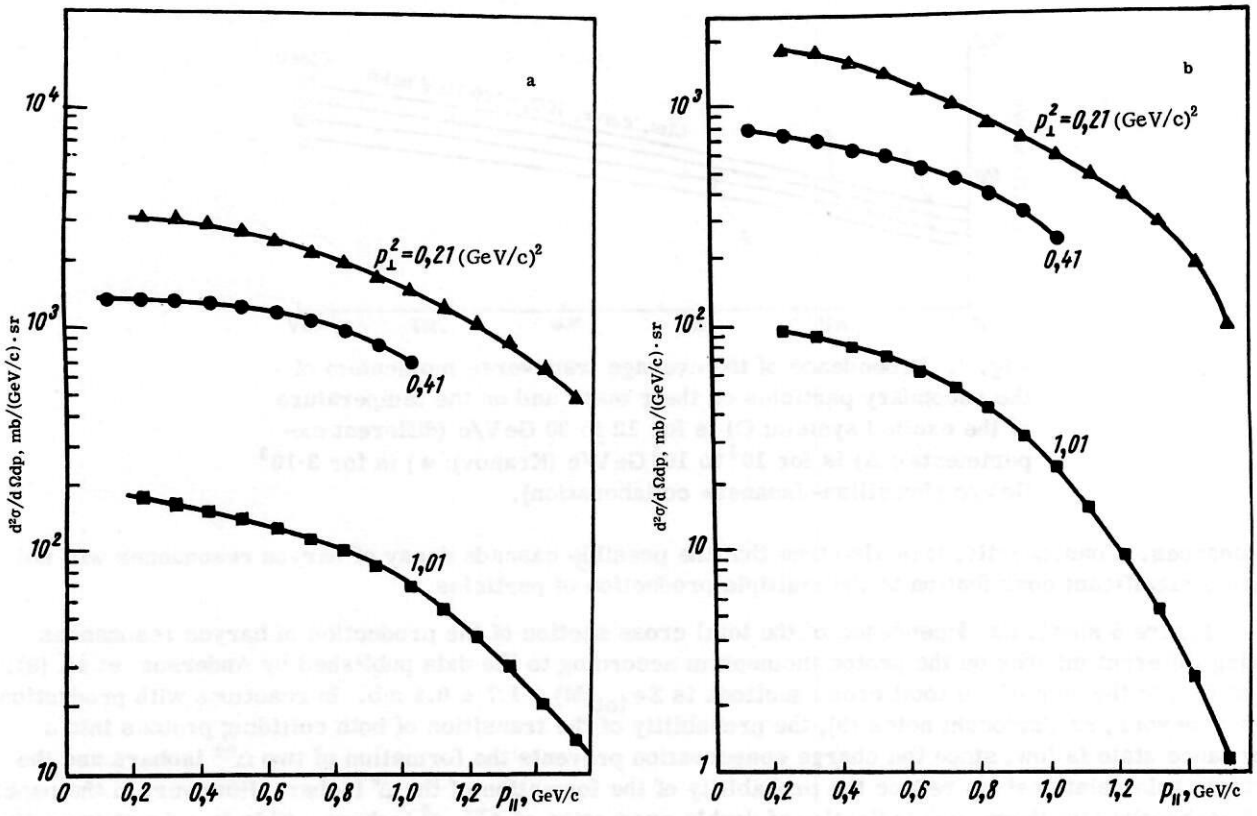

Fig. 9. Dependence of the differential cross section for the production of π^+ mesons (a) and π^- meansons (b) for fixed $p_\perp$ on the longitudinal momentum in pp collisions at 12.2 GeV/c in the center of mass system.

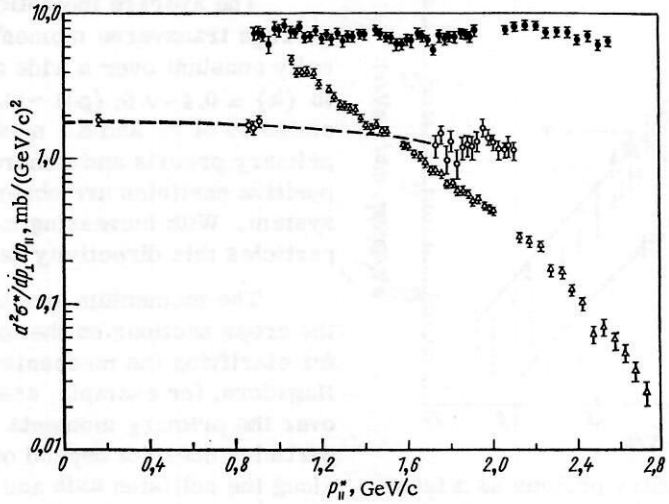

Fig. 10. Dependence of the differential cross section of the emission of secondary protons for $p_\perp^* = 0.18 \pm 0.02$ GeV/c (●); for $P_\perp^* = 1.0 \pm 0.04$ GeV/c (○) and π^- for $p_\perp^* = 0.18 \pm 0.02$ GeV/c (△) on $p_{||}^*$.

ture T ~ 120 MeV, and at higher (cosmic) energies T ~ 160 MeV. Hagedorn applies statistical thermodynamics, assuming the formation of highly excited blobs of hadron matter which decay in ~ 10^{-23} sec.

In [11] Hagedorn derived the following equations for the average magnitudes of the transverse momentum of the secondary particles as a function of their mass and temperature:

$$\langle p_\perp (m, T)\rangle = \sqrt{\frac{\pi m T}{2}} \cdot \frac{K_{5/2}\left(\frac{m}{T}\right)}{K_2\left(\frac{m}{T}\right)}, \tag{3}$$

where $K_{5/2}$, K_2 is the "K" function.

Figure 7 shows the experimental data and the values of $\langle p_\perp (m, T)\rangle$, calculated according to Eqs. (3). In the paper by Anderson [12] the dependence of the number of secondary protons on the transverse and longitudinal momentum $p_\parallel^*$ is obtained in the center of mass system. This dependence is expressed by the differential cross sections $d^2\sigma/dp_\perp dp_\parallel^*$, which are shown in Fig. 8 for three values of proton momentum: 10, 20, and 30 GeV/c. It turned out that the cross sections basically do not depend on $p_\parallel^*$, whose values varied in the range from 0.2 to 3 GeV/c. The experimental points in Fig. 8 may be described by empirical curves corresponding to the equation

$$\frac{d^2\sigma}{dp_\perp dp_\parallel^*} = 610 \cdot p_\perp \exp\left(-\frac{p_\perp}{0{,}166}\right) \frac{\text{mb}}{(\text{GeV/c})^2}. \tag{4}$$

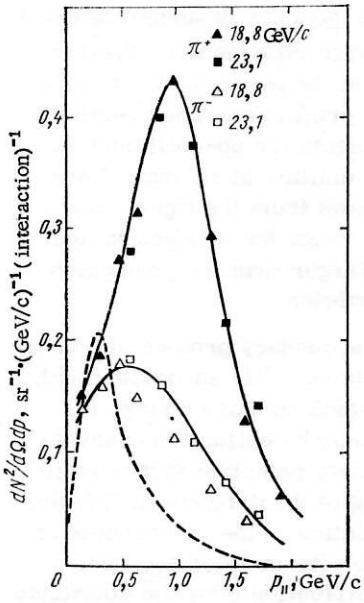

Fig. 11. Dependence of the differential cross section of $\pi^\pm$ mesons on the longitudinal momentum in the center of mass system in the case when the mesons were emitted at the angle 0° in the laboratory system (the dashed line is the statistical model).

Equation (4), after transformation to the variables p, θ (the momentum and angle in the laboratory system), takes the form

$$\frac{d^2\sigma}{dp\, d\Omega} = \frac{p^2}{2\pi} \cdot \frac{\gamma_c (E - \beta_c \cos\theta)}{E} 610 p_\perp \exp\left(-\frac{p_\perp}{0{,}166}\right) \frac{\text{mb}}{(\text{GeV/c})\text{sr}}, \tag{5}$$

which is similar to the dependence obtained by Hagedorn in statistical theory for central collisions. Figure 9 shows the dependence of the differential cross sections $d^2\sigma/dp_\perp\, dp_\parallel^*$ for production of pions from $p_\parallel^*$ for fixed values of $p_\perp$ in pp → $\pi\pm$M reactions, where M is the defect mass at 12.5 GeV/c. Figure 10 shows the dependence of the cross sections $d^2\sigma/dp_\perp \cdot dp_\parallel^*$ on $p_\parallel^*$ for fixed $p_\perp$. It follows from these reactions that for protons a strong dependence of the cross sections on $p_\perp$ and practically constant cross sections as a function of $p_\parallel^*$ are observed. For pions the cross sections drop almost by three orders when $p_\parallel^*$ varies in the $0.8 \leq p_\parallel^* \leq 2.8$ GeV range. Assuming that the uncertainty principle is valid with the equality sign in [13] in inelastic collisions of fast particles, the author derives the equation for the ratio between the dispersions of the longitudinal $\langle \Delta^2 p_\parallel^*\rangle^{1/2}$ and transverse momentum ($\langle \Delta p_\perp^2\rangle = \langle p_\perp^2\rangle$):

$$\frac{2\langle \Delta p_\parallel^{2*}\rangle^{1/2}}{\langle p_\perp^2\rangle^{1/2}} = \gamma_c, \tag{6}$$

where γ_c is the Lorentz factor of the center of mass system.

The use of Eq. (6) for protons and λ hyperons in πp collisions of of 7 GeV/c in the present paper, and likewise in [14], shows that Eq. (6) is valid within the limits of the experimental accuracy of ~ 10%. (Data on the dispersions $p_\parallel$ of the momenta in pp-collisions are unknown to the author). If Eq. (6) is valid, then inelastic collisions occur in such a

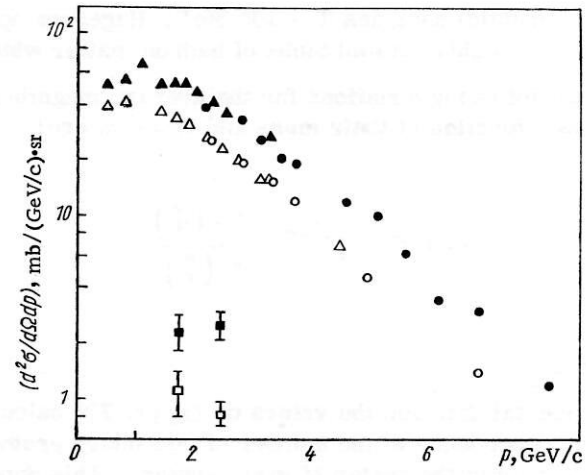

Fig. 12. Dependence of the production cross section for $\pi^{\pm}$ and $K^{\pm}$ mesons on their momentum if they are emitted at an angle 6°40' in the laboratory coordinate system in pp collisions at 19 GeV/c: △●) π^+; △○) π^-; ■) K^+; □) K^-.

way and in such a time that the Lorentz contradiction of the nucleons in the longitudinal direction does not change. The momentum spectrum of $\pi\pm$ mesons emitted at the angle 0° in thelaboratory system in pp-collisions at 19 and 23 GeV/c was measured in the paper by Dekkers [15]. The differential cross sections $d^2\sigma/dp\,d\Omega$ are shown in Fig. 11 as a function of the longitudinal momentum in the center of mass system. It follows from this figure that statistical theory does not describe the spectra of $\pi\pm$ mesons, and a specially large difference is observed for the π^+ meson. Figure 12 from the paper by A. D. Krisch [16] shows the dependence of the production cross sections of $\pi\pm$ and K± mesons on the momenta for pp-collisions at 19 GeV/c when the mesons were emitted at an angle 6°40' in the laboratory system. It follows from the figure that throughout the entire momentum range the production and rotation of positive particles is larger than the production and cross section of negative particles.

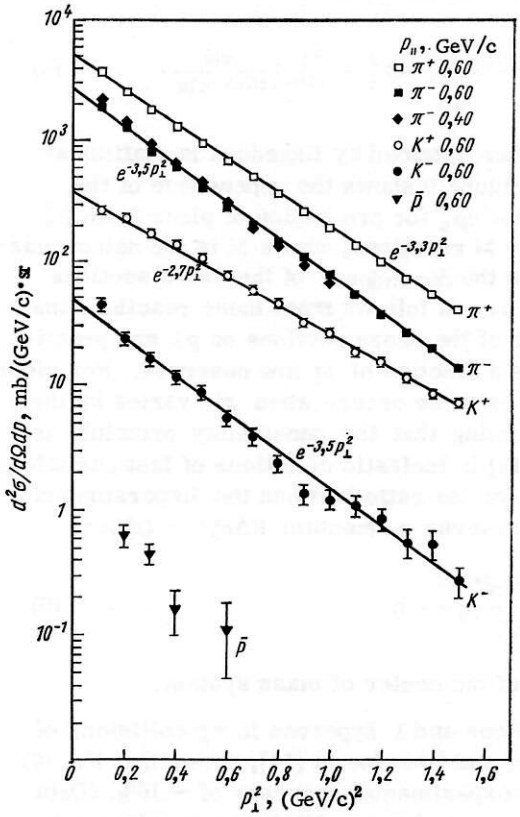

Fig. 13. Differential cross sections for various particles as a function of $p_\perp$ for fixed values of the longitudinal momentum in the center of mass system $p_{\parallel}^* = 0.4$ or 0.6 GeV/c.

The constancy of $\langle p_\perp \rangle$ for secondary protons allows the assumption to be made that this is possibly associated with the stability of the interaction region during a change in energy. The interaction region may be estimated quantitatively on the basis of the uncertainty principle if it is valid with the equality sign. According to W. Heisenberg [17] this is fulfilled for a Gaussian distribution of the components of the momenta and coordinates when the product $\Delta p_x \Delta x$ is minimized. If the momentum distribution over the coordinate axes x, y in a plane perpendicular to the trajectory of the impinging protons is Gaussian, then the distribution has the following form as a function of $p_\perp$:

$$dN(p_\perp) = cp_\perp \exp\left(-\frac{p_\perp^2}{\langle p_\perp^2 \rangle}\right) dp_\perp. \qquad (7)$$

If $p_{\parallel}^*$ is fixed, then $dp\,d\Omega = 2\pi \sec\theta\, d\theta\, dp_\perp$ and Eq. (7) is transformed to

$$\frac{d^2\sigma}{dp\,d\Omega} = c\cos\theta p_\perp \exp\left(-\frac{p_\perp^2}{\langle p_\perp^2 \rangle}\right). \qquad (8)$$

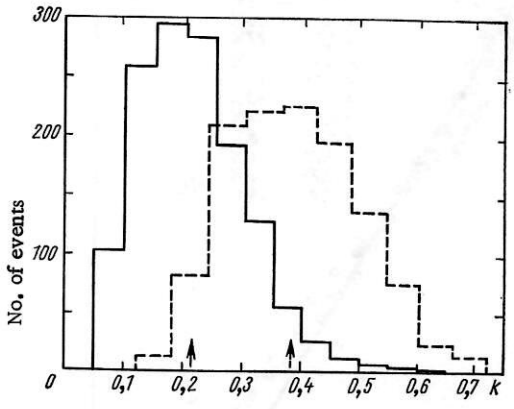

Fig. 14

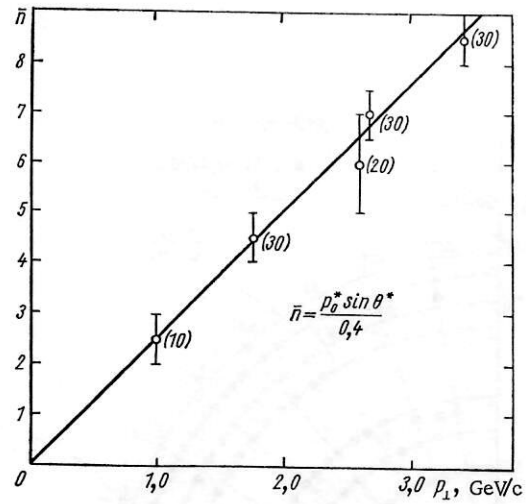

Fig. 15

Fig. 14. Dependence of the distribution of $pp \to \begin{cases} pp\pi^+\pi^-(-) \\ pp2\pi^+2\pi^- (- - -) \end{cases}$ events on the inelasticity factor k in collisions at 28.5 GeV/c.

Fig. 15. Dependence of the average number of pions on the transverse momentum of the secondary protons.

Figure 13 shows the functions $d^2\sigma/dp\,d\Omega$ for various secondary particles for fixed values of $p_{\parallel}^*$ which are equal to 0.6 and 0.4 GeV/c. The variation of $p_\perp$ takes place in the limit $0.45 \leq p_\perp \leq 1.3$ GeV/c, i.e., the factor $\theta p_\perp$ in Eq. (8) varies by approximately two orders, whereas $d^2\sigma/dp\,d\Omega$ in Fig. 13 is reduced by three orders. Consequently, in accordance with Eq. (8) the linearity in the logarithmic scale of the function $d^2\sigma/dp\,d\Omega$ in Fig. 13 corresponds to a Gaussian dependence of this function on the variable $p_\perp^2$.

For different secondary particles the functions $d^2\sigma/dp\,d\Omega$ have a closely similar slope: $d^2\sigma/dpd\Omega \sim e^{-3,3p_\perp^2}$, i.e., the parameter $\langle p_\perp^2 \rangle$ in Eq. (8) is the same. In accordance with the uncertainty principle this indicates that all the particles are emitted from one region. On this subject, A. D. Krisch [16] comments: this is strange, since K± and $\tilde{p}$ have a large mass, but it is evidently true.

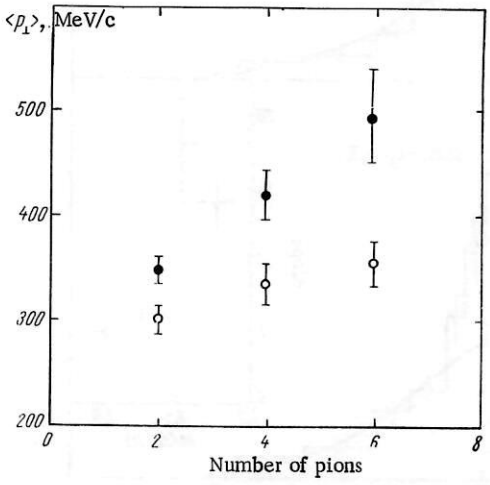

Fig. 16. Dependence of $\langle p_\perp \rangle$ for protons (●) and π mesons (○) on the number of produced mesons in collisions at 28.5 GeV/c.

Let us note that this regularity is in accord with that considered in Secs. 1.1 and 1.2 of the paper by P. Rotelly.

Purposeful work on the investigation of cross sections and momenta was carried out at the Argonne Laboratory. In the paper by A. D. Krisch [16] the dependence $d^2\sigma/dpd\Omega\ (p_\perp^2)$ was investigated for secondary protons by registering their total momentum at the center of mass system (i.e., for a condition analogous to elastic scattering). It was found that at large angles $p_c = 2.1$ GeV/c the elastic and inelastic cross sections have an identical slope: $d\sigma/d(-t) \propto d^2\sigma/dpd\Omega \sim e^{-3p_\perp^2}$. Consequently, the break in the slope of the graph for the inelastic cross sections (i.e., the growth of the parameter $\langle p_\perp^2 \rangle$ in Eqs. (7) and (8)) takes place by analogy with the case of elastic scattering (see Ch. 2).

In the paper by Ashbury [18] the production of $\pi\pm$-mesons in pp collisions at 12.5 GeV/c were investigated. It was found that for a longitudinal momentum $p_{\parallel}^* = 0.6$ GeV/c which is fixed in the center of mass system the cross sections $d^2\sigma/dpd\Omega\ (p_\perp^2)$ have a break and can be described by two or more Gaussian functions. These regularities are possibly associated with the change in the interaction region when the transition is made to higher values of $p_\perp$. This is

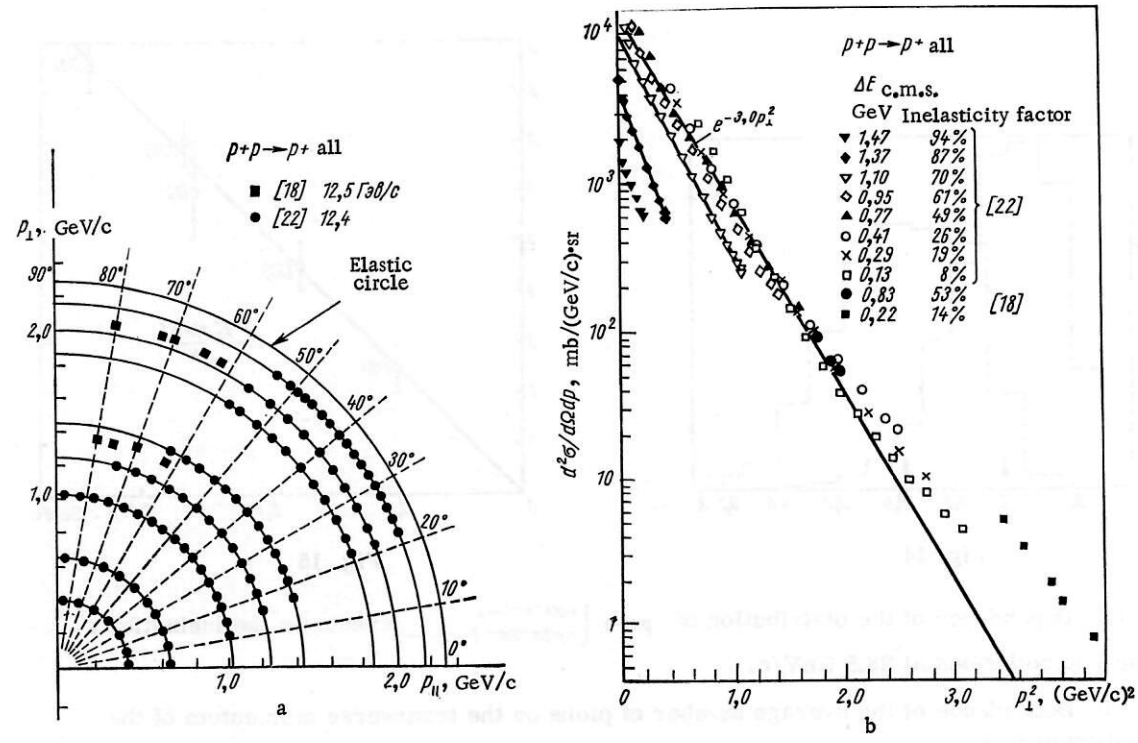

Fig. 17. The measurement conditions (momenta and angles in the center of mass system) for fixed inelasticity factors (a) and the dependence of the cross section $d^2\sigma/dp\,d\Omega$ on $p_\perp^2$ for various values of the inelasticity factor (b).

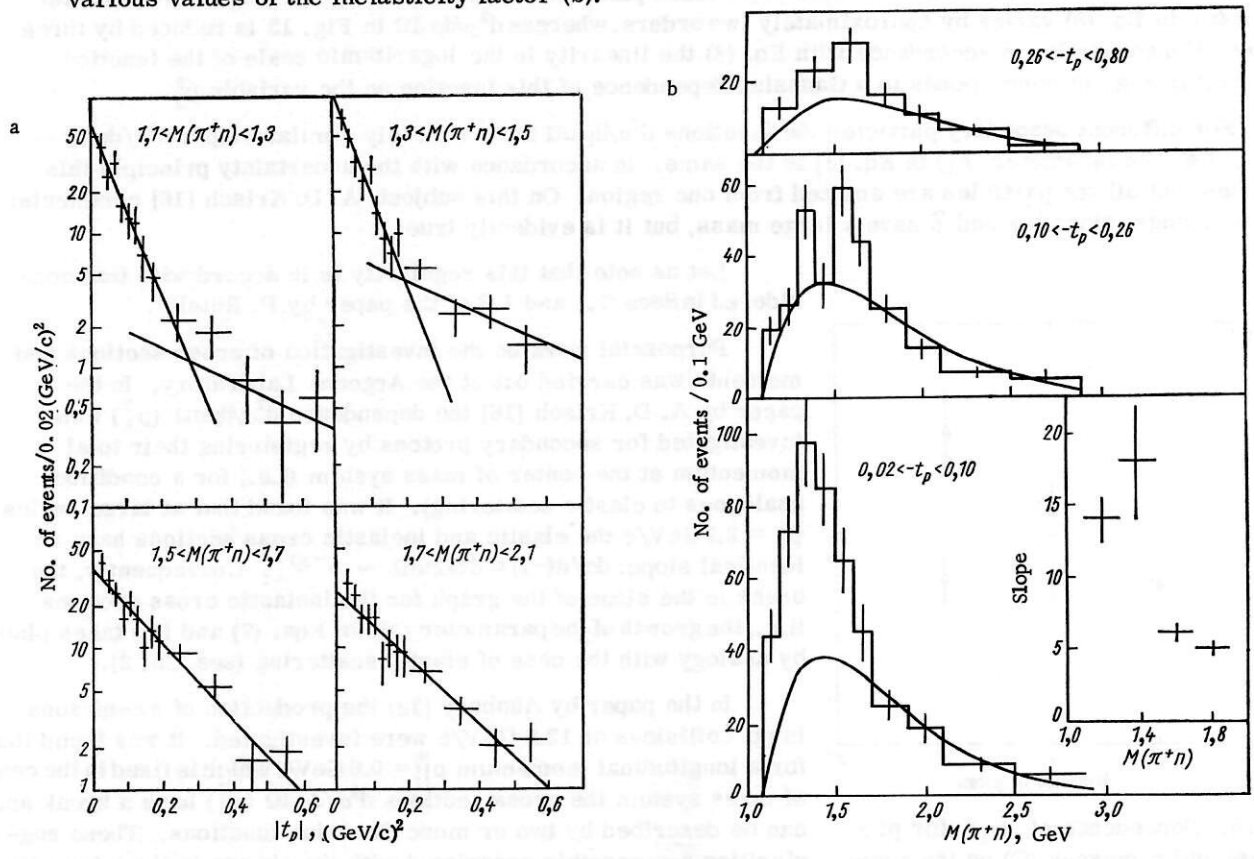

Fig. 18. Distribution of events for various intervals of the $n\pi^+$ masses as a function of the square of the transferred 4-momentum $|t_p|$ at 28.5 GeV/c in the $pp \to pn\pi^+$ reaction (a), and mass distribution in the $pp \to pn\pi^+$ reaction (b).

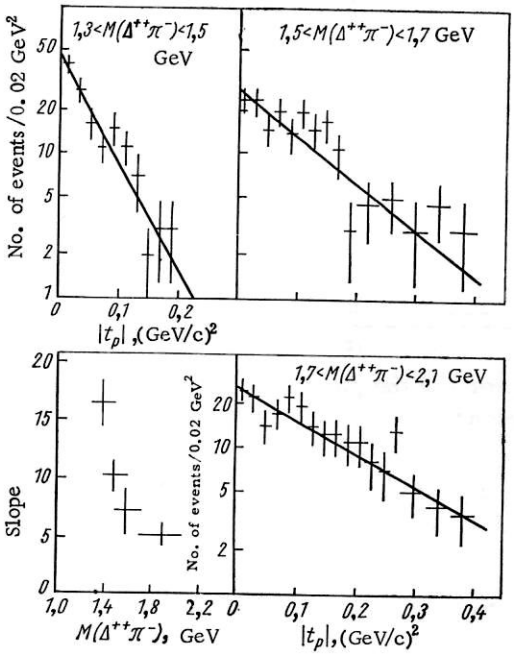

Fig. 19. Dependence of the distribution of events for various mass intervals of the $\Delta^{++}\pi^-$ system on $|t_p|$ in the pp → $p\Delta^{++}\pi^-$ reaction at 28.5 GeV/c.

likewise indicated by the relationships between the inelasticity coefficients, the multiplicity of π-mesons and $p_\perp$. Figure 14 shows the result obtained by P. Connally reported in [19] which indicates a growth of almost a factor of two in the averaged inelasticity factor for the number of $\pi\pm$- mesons in the pp → $pp\pi^+\pi^-$ and pp → $pp\pi^+\pi^+\pi^-\pi^-$ directions at 28.5 GeV. In the paper by E. V. Anderson [20] processes characterized by a high inelasticity factor are considered at three values of primary energy, 10, 20, and 30 GeV, and a growth of the average number of pions with increasing $p_\perp$ of the secondary protons is indicated. The results are displayed in Fig. 15, and the authors explain them in the spirit of the "bremsstrahlung" model of Lewis, Oppenheimer, and Votazin. In this model, and likewise in the paper by Kastrup [21], a relationship was found between the emission angle of the proton and the multiplicity of the mesons.

In Fig. 16 from [19] the dependence of $\langle p_\perp \rangle$ for protons and mesons on the multiplicity of π-mesons is shown for pp-collisions at 28.5 GeV, and a substantial growth of $\langle p_\perp \rangle$ is observed for protons with an increase in the number of mesons.

In aggregate the results enumerated are in agreement with the proposition that the average inelasticity factor increases (and, consequently, the number of secondary particles likewise increases) for an increase in the average transverse momentum (i.e., for a decrease of the "impact parameter").

However, the relationship between the average magnitude of the transverse momentum and the inelasticity factor K does not convey the details of the interaction. Actually, the investigations performed in the work by Day [22] indicate a more complex link between K and $p_\perp$. In that work the differential cross sections were measured in a wide range of scattering angles for pp-collisions at 12.4 GeV/c while registering the values of K in individual series of measurements; these values, in turn, were varied within the limits $0.08 \leq K \leq 0.94$. The conditions for these experiments are illustrated by Fig. 17a, while Fig. 17b shows the momenta of the secondary protons corresponding to various K.

It was found that in the range $0.08 \leq K \leq 0.62$ the absolute values of the cross sections $d^2\sigma/dp\,d\Omega$ in the center of mass system are close to being constant for fixed values of $p_\perp$. This can be seen from Fig. 17b where for various K the points showing the cross sections $d^2\sigma/dp\,d\Omega$ are superimposed on each other. Consequently, in the range $0.08 \leq K \leq 0.62$ the quantity $p_\perp$ does not depend on K. In contrast to this the the cross sections $d^2\sigma/dp\,d\Omega$ decreases with an increase in K in the range $0.7 \leq K \leq 0.94$.

Further on it is clarified that for various K the dependence of the cross sections on $p_\perp$ have the form

$$\frac{d^2\sigma}{dp\,d\Omega}(p_\perp) \sim \exp(-3p_\perp^2),$$

i.e., in accordance with Fig. 13 it is close to the dependence of analogous cross sections for various secondary particles. Consequently, similar regularities are manifested in the spectra of the protons and the produced particles.

1.6. Quasi-two-particle Processes

Quasi-two-particle processes are more probable at a high multiplicity of the secondary particles.

Chan Hong Mo [23] considers that the separation between two-particle and multiparticle processes is basically artificial and is merely a historical relic. This conclusion is based on the fact that without knowing the dynamics of hadron collisions one cannot subdivide events according to multiplicity, by analogy with the fact that the subdivision of interactions into peripheral and central interactions was never assured (in the experimental sense) by its original content. However, the singling out of quasi-two-particle processes is justified from the experimental standpoint by the fact that for the time being more complete data

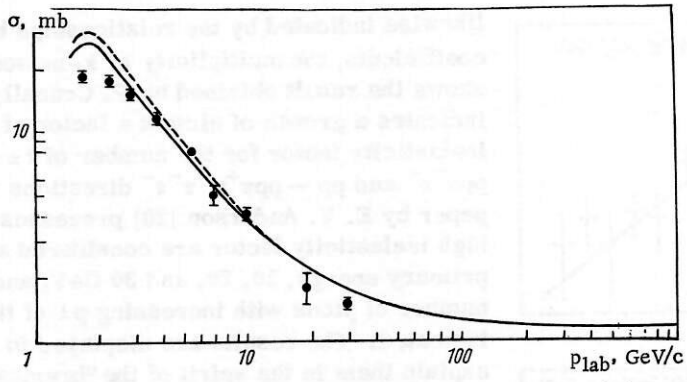

Fig. 20. Dependence of the total cross section of the $pp \to pn\pi^+$ reaction on the momentum of the protons.

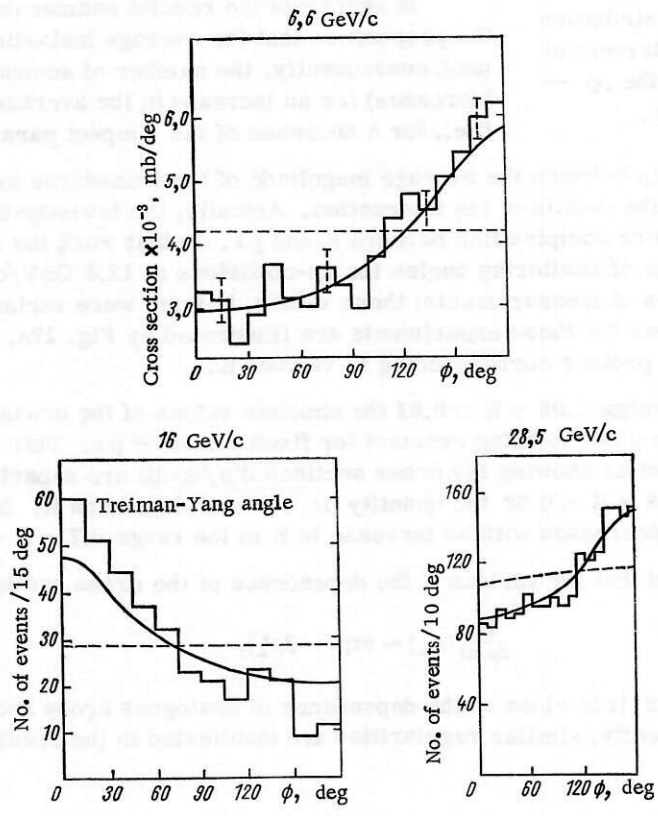

Fig. 21. Distribution of events over the Treiman-Yang angles in $pp \to \Delta^{++}p\pi^-$ reactions (the solid line corresponds to the Regge model; the dashed line corresponds to the one-pion model).

TABLE 1. Dependence of the Parameters a, b, c on the Primary Momentum

Prim. momentum, GeV/c; 4-momentum t, $(GeV/c)^2$	a	b, $(GeV/c)^{-2}$	c, $(GeV/c)^{-4}$	Literature
15,1 $0,22 < -t < 0,78$	4,08±0,14	7,89±0,59	−0,43±0,59	[26]
18,4 $0,2 < -t < 0,5$	4,18±0,08	8,58±0,24	—	[27]
19,84 $0,2 < -t < 0,8$	4,19±0,15	8,68±0,79	0,70±0,92	[28]
20,0 $0,21 < -t < 0,8$	4,23±0,10	9,15±0,45	0,72±0,45	[26]
24,63 $0,25 < -t < 0,75$	4,09±0,30	7,97±1,56	0,82±1,83	[28]
29,7 $0,21 < -t < 0,73$	3,76±0,12	8,02±0,60	−0,64±0,65	[26]

can be obtained at a lower multiplicity. Experiments show that an analogy with elastic scattering is observed – each of the colliding particles has a tendency to transfer the state of its motion to the corresponding final particle. Further, the excitation energy is small, as well as the 4-momentum transfer. Therefore, at high energies reactions of this type are likewise called quasielastic scattering.

In the paper by Bertocchi [9] it is noted that the dynamic causes of this similarity are completely different. In elastic scattering this is basically a consequence of the diffraction pattern. In quasielastic scattering there is no diffraction, and the observed predominance of 4-momentum transfers having a small absolute magnitude is of dynamic origin as a consequence of another interaction mechanism.

For the $pp \to pn\pi^+$ reaction at 28.5 GeV the distribution of events as a function of the transferred 4-momentum $-t_p$ of a proton is displayed in Fig. 18a for various mass intervals of the $n\pi^+$ system. In the first two mass intervals the distribution with respect to t_p may be represented by $\sim \exp(18t_p)$, breaks being observed at $-t_p \sim 0.3$ $(GeV/c)^2$.

Figure 18b gives the distribution over the effective masses of $n\pi^+$ and the slopes for small $|t|$ as a function of the mass of $n\pi^+$.

Figure 19 displays analogous distributions for the $pp \to p\Delta^{++}\pi^-$ reaction at 28.5 GeV/c also, as well as the slope of the distribution with respect to t_p as a function of the mass of $\Delta^{++}\pi^-$. It follows from Figs. 18 and 19 that the slope decreases when the transition is made to large masses of the system $n\pi^-$ and $\Delta^{++}\pi^-$.

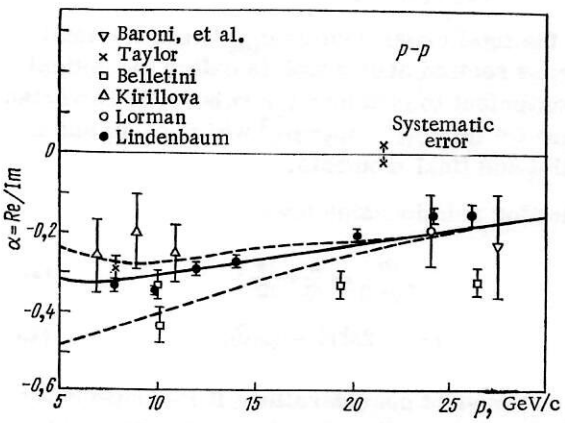

Fig. 22. Dependence of the ratio between the real part of the scattering amplitude and the imaginary part on momentum.

For small values of $|t|$ it may be assumed that $-t \sim p_\perp^2$, and a comparison with Eq. (7) shows that the reduction of the slope with increasing mass corresponds to an increase of $\langle p_\perp^2 \rangle$ (i.e., a reduction of the "impact parameter"). In order to substantiate this conclusion it is necessary to use the data on the dependence of the processes described on the angular momenta.

Events having a low multiplicity of secondary particles in the low-energy range have been explained successfully by the model with exchange of one pion (OPM). In the energy range which is fairly far from the threshold of baryon resonances the Satz paper [24] carries out a calculation of the cross sections of the $pp \to pn\pi^+$ reaction on the basis of the OPM; however, it uses the experimental values of the transferred momentum.

Figure 20 presents the results of this calculation. A difference from experimental data is observed at low proton momenta and in the ~ 30 GeV/c region where the reaction cross section is already less than 1 mb.

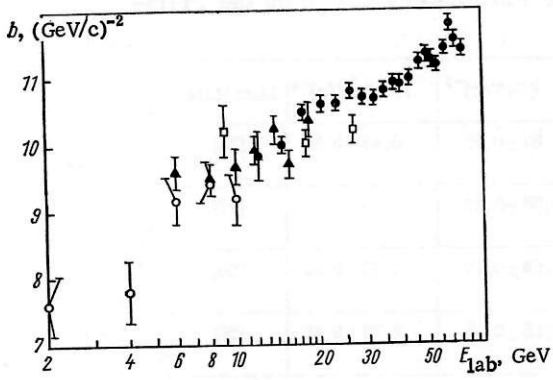

Fig. 23

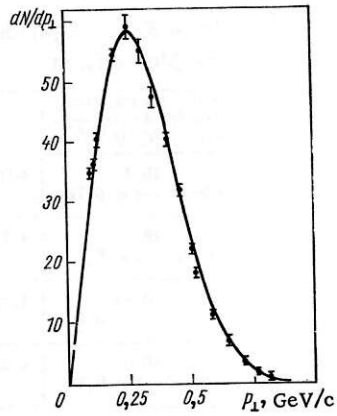

Fig. 24

Fig. 23. Dependence of the slope parameters b on proton energy.

Fig. 24. $dN/dp_\perp(p_\perp)$ in elastic pp collisions at 11 GeV/c.

In describing a number of phenomena good agreement with experiment is obtained on the basis of the Regge model. This is evident, for example, in Fig. 21 where histograms of the distributions with respect to the Treiman-Yang angles and calculations according to the Regge and OPM models are presented for the $pp \to \Delta^{++}p\pi^-$ reaction at 6.6, 16, and 28.5 GeV/c.

II. ELASTIC pp-SCATTERING

The general case is complexity of scattering matrix T = D + iA. For elastic scattering of fermions the differential cross section is related to T by the equation

$$\frac{d\sigma}{d\Omega} = \frac{1}{4\pi^2} \cdot \frac{m^2}{S} T^2, \tag{9}$$

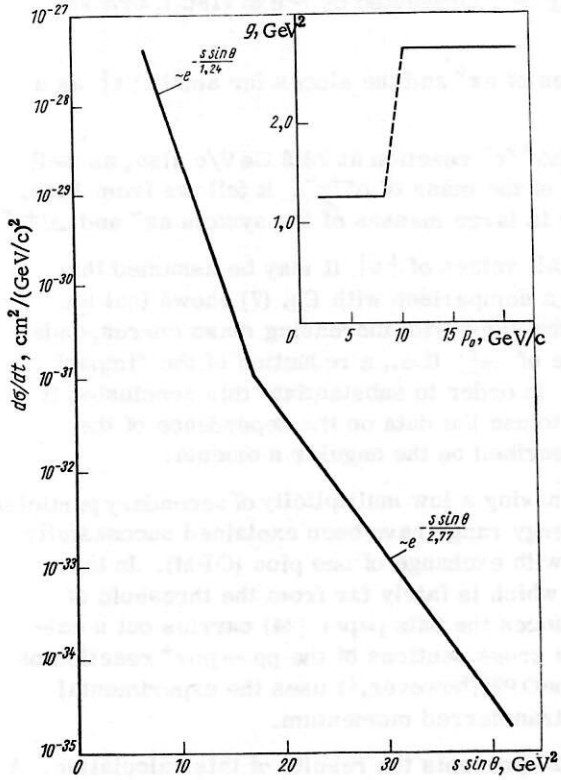

Fig. 25. $d\sigma/dt\,(s\cdot\sin\theta)$.

where $S = (p_1 + p_2)^2$ is the square of the total energy in the center of mass system. For zero-angle scattering:

$$\left(\frac{d\sigma}{d\Omega}\right)_{\theta=0} = \frac{1}{4\pi^2} \cdot \frac{m^2}{S}(D^2 + A^2). \tag{10}$$

If the real part D of the scattering amplitude is zero, then we obtain the equation

$$\left(\frac{d\sigma}{d\Omega}\right)_{\theta=0} = \left(\frac{p_c \sigma_{tot}}{4\pi}\right)^2, \tag{11}$$

which relates the total cross section σ_{tot} to the minimal differential cross section at 0° which is called the optical value. It is convenient to consider the relativistic invariant $d\sigma/d(-t)$, where $t = (p_1 - p_1')^2 = (p_2 - p_2')^2$ where p_1', p_2 and p_1', p_2' are the initial and final momenta.

The following relationships hold:

$$\frac{d\sigma}{d(-t)} = \frac{\pi}{p_c^2} \cdot \frac{d\sigma}{d\Omega}; \tag{12}$$

$$t = -2p_c^2(1 - \cos\theta). \tag{13}$$

For the subsequent considerations it is convenient to separate the ranges of small and large scattering angles, and likewise to isolate the angles ~ 90°.

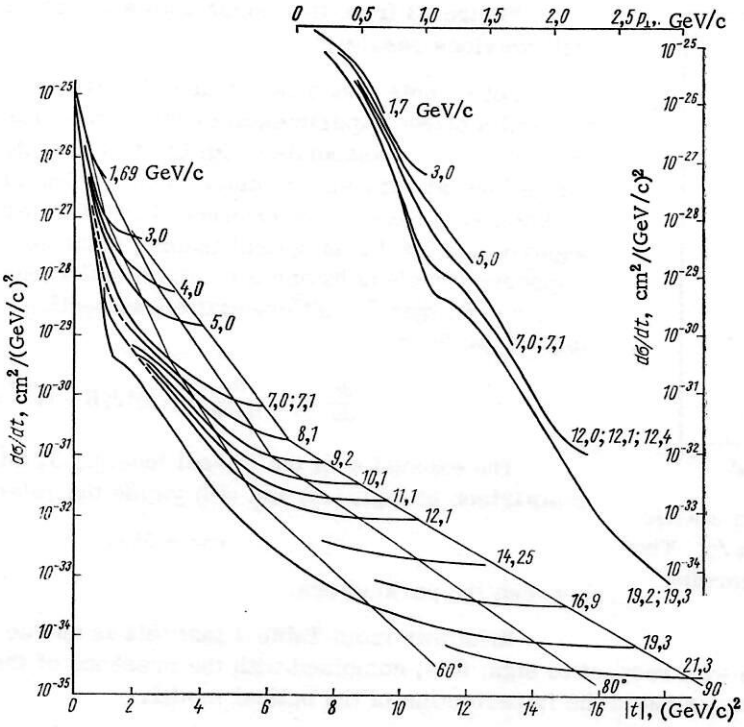

Fig. 26. $d\sigma/dt$ ($|t|$) in elastic pp scattering.

2.1. Small-Angle Scattering

A comparison of the experimental values of the differential cross sections near 0° with those calculated according to Eq. (11) allows a conclusion to be drawn concerning the real part of the scattering amplitude. The first indications of the presence of a real part were obtained on the synchrophasotron at the High-Energy Laboratory [25]. For extrapolation of the differential cross sections to a zero angle an excess above the optical cross section was obtained which corresponded to a ratio ~ 0.7 ± 0.2 between the real part of the potential and the imaginary part. Currently known values of the magnitude of the ratios $\alpha(S)$ of the real part of the scattering amplitude to the imaginary part are given in Fig. 22.

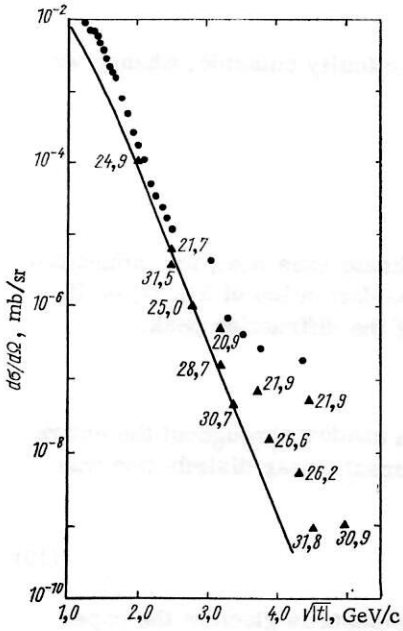

Fig. 27. $d\sigma/d\Omega$ ($|t|$) in elastic pp scattering.

If the scattering angles are still not very small (i.e., interference between the Coulomb scattering amplitude and the real part of the nuclear-scattering amplitude is negligible), then from Eq. (10) and Fig. 22 it follows that at energies ~ 10 GeV the contribution from the real portion of the amplitude to the cross section is ~ 0.1.

The cross sections $d\sigma/d(-t)$ (t) in the range of small values of $|t|$ may be described by the phenomenological equation:

$$\frac{d\sigma}{d(-t)} = \exp(a + bt + ct^2). \qquad (14)$$

In [26–28] values of the parameters b and c were obtained which are given in Table 1.

Measurements of the parameter b were carried out by G. G. Beznogikh [29] on the Serpukhov accelerator in the energy range from 12 to 70 GeV at very high values of $|t|$:

$$0{,}01 \leqslant |t| \leqslant 0.12 \text{ (GeV/c)}^2.$$

The dependence of b on the energy is expressed by the author using the formula:

$$b = \left[(6.8 \pm 0.3) + (0.94 \pm 0.18) \ln \frac{s}{s_0}\right] \text{(GeV/c)}^2. \qquad (15)$$

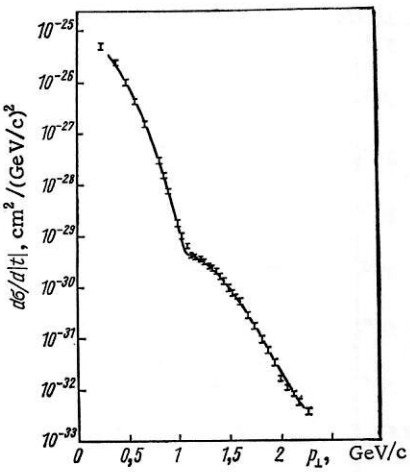

Fig. 28. $d\sigma/d|t|$ ($|t|$) in elastic pp scattering at 19.2 GeV/c. The curve was calculated according to Eq. (24).

Figure 23 from that paper ahows the results obtained along with previous results.*

Let us note that these values of b are somewhat higher (within the limits of two experimental errors) than those previously known. Possibly, this is associated with the fact that the measurements were carried out at very small values of $|t|$. The growth of the parameter b with energy causes a narrowing of the diffraction peak, since t is negative and $c \ll b$. In optical theory, if the scattering is produced by a spherical nucleus having a radius R and a transparency coefficient a for $r < R$, then for differential cross sections of scattering at an angle θ we have

$$\frac{d\sigma}{d\Omega}(\theta) = \frac{R^2}{\sin^2\theta}(1-a)^2 J_1^2[(-t)^{1/2} R]. \tag{16}$$

The expansion of the Bessel function J_1 into a series and the comparison of Eqs. (14) and (16) yields the relationship

$$c = -b^2/12$$

between the parameters.

It follows from Table 1 that this is untrue not only with respect to the magnitude but also with respect to sign; this, combined with the presence of the real part of the scattering amplitude, demonstrates the imperfection of the optical model.

In papers by the author [30, 31] Eq. (7) was used to describe the differential cross sections of elastic scattering in the region of the diffraction peak. Figure 24 shows the curve calculated according to Eq. (7) for pp scattering at ~ 11 GeV/c when $< p_\perp^2 >^{1/2} = 0.35$ GeV/c. The experimental points in Fig. 24 have been plotted according to the data given in the papers by L. S. Kirillova [32] and Foley [33]. Using the relationships

$$p_\perp^2 = -t + \frac{t^2}{4p_c^2}, \tag{17}$$

Eq. (7) may be transformed to

$$\frac{d\sigma}{d(-t)} = c \exp\left(\frac{t + \frac{t^2}{4p_c^2}}{\langle p_\perp^2 \rangle}\right)\left(1 + \frac{t}{2p_c^2}\right). \tag{18}$$

At small $|t|$ the factor $1 + (t/2p_c^2)$ is negligible, and Eqs. (14) and (18) practically coincide, whence we obtain the relationships

$$c = \frac{b}{4p_c^2}$$

between the parameters.

Thus, assuming a Gaussian spectrum of the momenta along the coordinate axes (i.e., the momentum distribution corresponding to the law for the case which was the basis of the derivation of Eq. (7) or its analog (18)) it is possible to describe the experimental data in the region of the diffraction peak.

2.2. Large-Angle Scattering

Elastic scattering must accompany the inelastic processes just like a shadow throughout the entire range of angles. In the range of large scattering angles the so-called universal Orear distribution was initially used extensively:

$$\frac{d\sigma}{d(-t)} = A \exp\left(-\frac{p_\perp}{a}\right), \tag{19}$$

*A comparisonwith calculations based on the theory of complex angular momenta is given in the paper by K. A. Ter-Martirosyan [30].

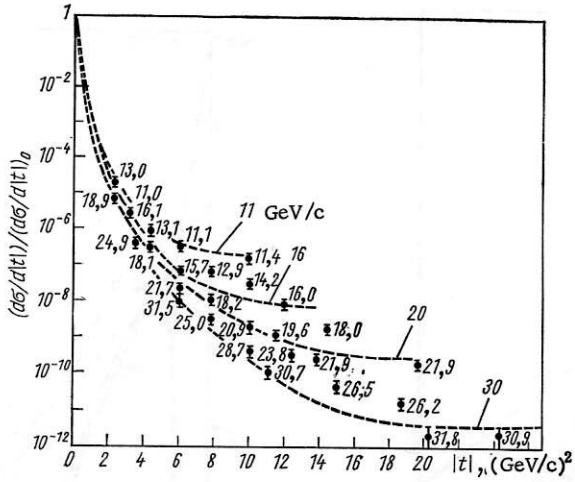

Fig. 29. $(d\sigma/d|t|)/(d\sigma/d|t|)_0$ as a function $|t|$ for elastic pp scattering at various energies.

in which $a \sim 160$ MeV/c. It was likewise used to describe two-particle reactions. With a refinement of the experimental data breaks in the distribution of $d\sigma/d\Omega$ (Akerlof [34]) appeared on the straight line in the logarithmic scale, and the equation

$$\frac{d\sigma}{d(-t)} \sim \exp\left(-\frac{s\sin\theta}{g}\right) \tag{20}$$

was used to describe them. Figure 25 shows the application of Eq. (20) to the description of the data from the papers by Ankenbrandt [35] and Allaby [36]. However, as the experimental data became more refined a "finer structure" was revealed as a function of $[d\sigma/d(-t)](t, s)$, which cannot be described by Eqs. (19) or (20) or their modifications. Figure 26 shows the results of experiments of many groups of authors which were performed over wide ranges of t and s, and taken from the Allaby paper [37]; here the dependence of $d\sigma/d(-t)$ is expressed in the variables $p_\perp$ and $t_\perp$.

In order to explain large-angle scattering a number of models have been advanced. In the paper by Wu [38] a decrease of the cross sections with increasing p, as well as the presence of excitation models of a nucleon having an energy above 300 MeV, is associated with the difficulty of imparting a large transverse momentum to the nucleon without "breaking it." Kinoshita [39] relates large-angle scattering to the condition requiring minimal scattering amplitude in accordance with the analyticity requirement. This treatment was continued by Martin [40]. He showed that calculations based on the nucleon form factor as proposed by Wu and Yang are in agreement at large $|t|$ with the fastest asymptotic reduction allowed by analyticity and the boundary conditions.

In papers by V. R. Garsevanishvili [41] a relativistic model of scattering events at high energies is considered which is based on the A. A. Logunov and A. N. Tavkhelidze quasipotential equation [42] for the scattering amplitude in quantum field theory. In this model the scattering of hadrons may be described by a smooth complex potential $V(\bar{r}, E)$, which depends on energy and is a nonsingular function of the relative coordinate $\bar{r}$. The imaginary part of this potential is caused by inelastic processes. This assumption means that the scattering may be treated as an interaction between two "loose" systems.

Let us introduce the simplest nonsingular quasipotential of the Gaussian type:

$$V(s, \bar{r}) = iSg_0\left(\frac{\pi}{a}\right)^{3/2} e^{-\frac{r}{4a}},$$

in which $g_0 > 0$, while the parameter a determines the effective interaction region and in the general case cannot increase more rapidly than $|a| \leq \ln s$, $s \to \infty$ with increasing energy. This potential ensures a constant total cross section at high energies.

The calculations were carried out for the range of small angles on the assumption that $|t/s| \ll 1$, as $\gg 1$. For large fixed angles the condition $|t/s| \simeq \sin^2(\theta/2)$ was used. The equation

$$\frac{d\sigma}{d\Omega} = \left(\frac{\pi a}{3}\right)^2 q^2 e^{-2q\sqrt{\pi a}} \tag{21}$$

was derived in which $q = \sqrt{|t|}$.

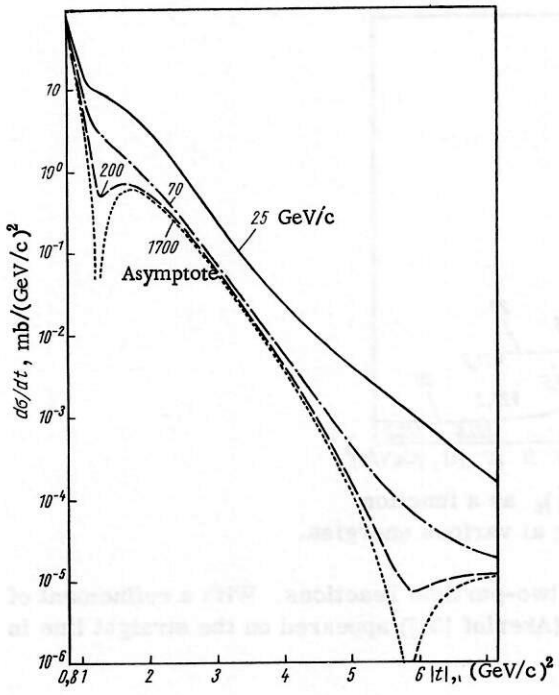

Fig. 30

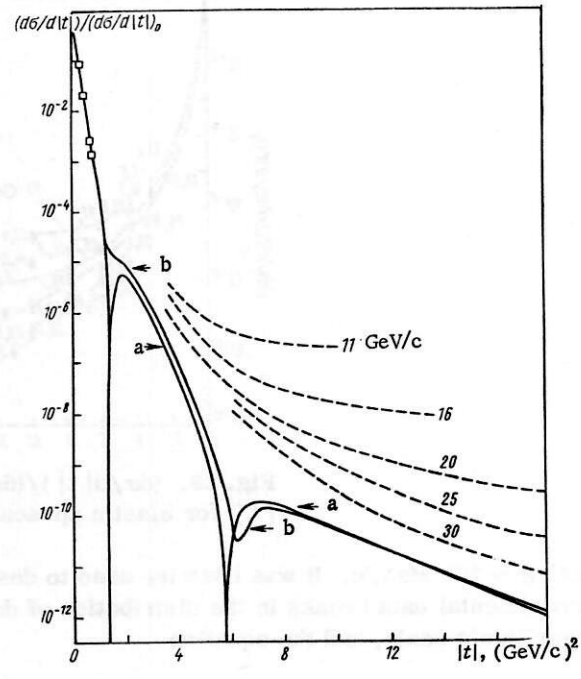

Fig. 31

Fig. 30. $d\sigma/d|t|$ as a function of $|t|$, calculated according to the hybrid model [50].

Fig. 31. $d\sigma/d|t|/(d\sigma/d|t|)_0$ as a function of $|t|$ according to the data of [51] (a) and [52] (b).

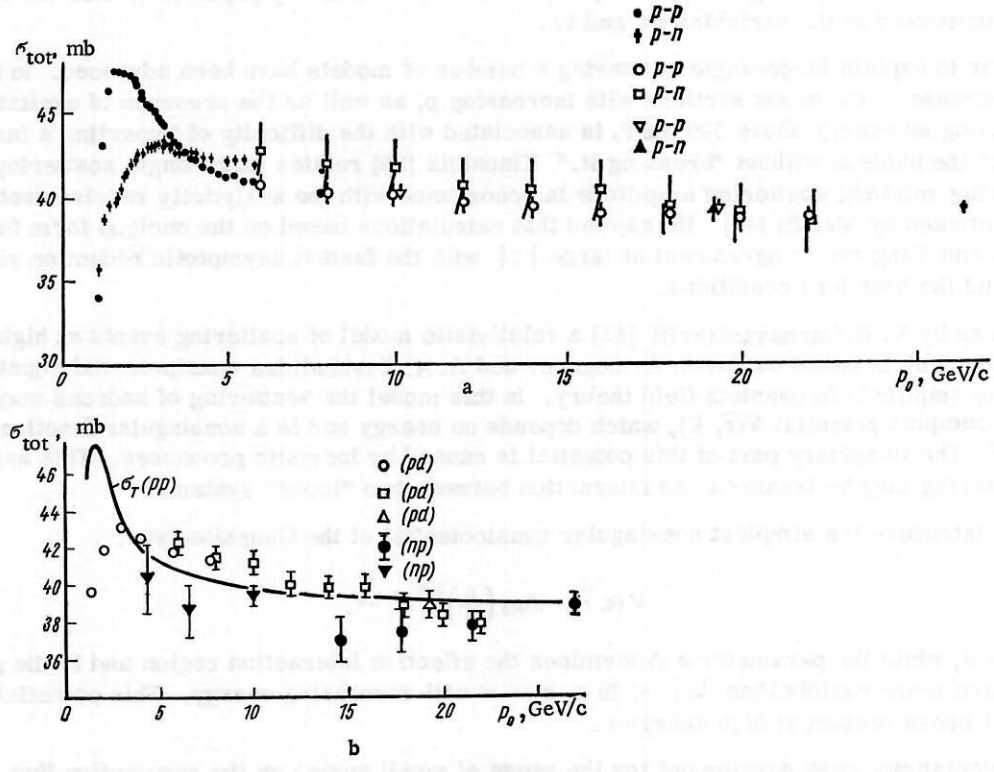

Fig. 32. Dependence of the total cross section of pp scattering (a) and np scattering (b) on the momentum.

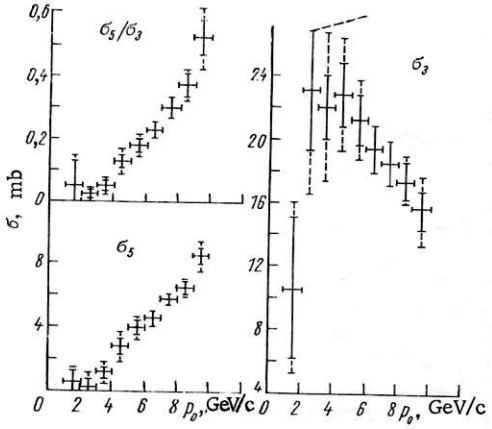

Fig. 33. Dependence of the cross section for the production of three and five charged particles in collisions on the primary momentum.

A peculiarity of Eq. (21) resides in the fact that for fixed momentum transfers at large scattering angles $d\sigma/d\Omega$ depends weakly on energy and only via the parameter a. This parameter is related to the width of the diffraction peak at small angles. Figure 27 shows the experimental data and the curves calculated according to Eq. (21) for $a = 3.0$ (GeV/c)^2, the authors noting that Eq. (21) is not applicable to angles $\sim 90°$.

In the papers by Ansel'm [43] large-angle scattering of protons was considered on the basis of the theory of complex angular momenta, and the resulting equation shows a drop of the cross section which is close to the Orear empirical dependence: $d\sigma/d|t| \sim e^{-p_\perp/a}$, where the parameter $a \approx 140$ MeV if $\sqrt{\ln(s/4m^2)} \sim 2$. Further on it is shown that for scattering angles $\theta < 60-65°$ the experimental data at different energies may be described approximately by the linear dependence

$$-\ln\left[\frac{d\sigma}{d|t|}\Big/\left(\frac{d\sigma}{d|t|}\right)_0\right] = 3.5\,(1+\sqrt{\tau\xi}),$$

where $\xi = \ln(s/4\ \text{GeV})^2$, $\tau = -t/1\ \text{GeV}^2$. For stipulated τ the values of $-\ln[d\sigma/d|t|/(d\sigma/d|t|)_0]$ depend fairly essentially on ξ, which qualitatively substantiates the theoretically predicted logarithmic energy dependence ($\sim \sqrt{\xi}$) of the exponent of the exponential drop of the cross sections with respect to $\sqrt{\tau}$.

Then we find that the equation for $d\sigma/d|t|$ includes oscillation terms containing (τ, ξ). Oscillations in the differential cross sections were likewise obtained in the paper by I. V. Andreev [44] in which the authors started from the shape of the diffraction peak and the unitarity condition for the scattering amplitude, which is taken in the form $A(p, \theta) = I_2 + F(p, \theta)$, in deriving the equation for large-angle scattering. Here

$$I_2 \quad \frac{1}{32\pi^2}\int\int d\theta_1\, d\theta_2 \frac{\sin\theta_1 \sin\theta_2\, A(p, \theta_1)\, A^*(p, \theta_2)}{\{[\cos 0 - \cos(\theta_1+\theta_2)][\cos(\theta_1-\theta_2)-\cos\theta]\}^{1/2}}, \qquad (22)$$

where p, θ are the momentum and scattering angle in the center of mass system; the integration domain is $|\theta_1-\theta_2| < \theta$; $\theta < (\theta_1+\theta_2) < 2\pi-\theta$.

The function $F(p, \theta)$ describes the contribution of inelastic processes to the elastic-scattering amplitude. The authors use the approximation in which the scattering amplitude is considered to be purely imaginary throughout the entire region of the diffraction cone $\theta < \theta_d$, while the amplitude normalization corresponds to the optical theorem:

$$\operatorname{Im} A(p, 0)_{\theta=0} = 4p^2\sigma_t.$$

Assuming for $\theta < \theta_d$ that $A(p, \theta) \approx 4ip^2\sigma_{tot}\, e^{-a p^2\theta^2/2}$ and substituting this expression into (22), one may confirm the fact that the two-particle contribution I_2 has a less abrupt angular dependence than does $\operatorname{Im} A(p, 0)/I_2 \sim \exp(-a^2p^2\theta^2/4)$. This means that for $\theta < \theta_d$ the principal contribution to $\operatorname{Im} A(p, \theta)$ is made by the function $F(p, \theta)$. Consequently, the presence of a two-particle contribution in the unitarity condition must lead to a weaker fall-off of the amplitude with increasing angles, which is what is observed.

In the ranges of angles $\theta \gg \theta_d$ it is assumed that $\operatorname{Im} A(p, \theta) \gg F(p, \theta)$, but that in a certain range of angles one still may not neglect $F(p, \theta)$. As a result the authors obtained the following equations for the logarithm of the differential cross section:

$$\ln\left(\frac{d\sigma}{d\Omega}\Big/c\right) \approx -2\sqrt{2a\ln(4\pi a/\sigma_{tot})}\,p\theta + 2\frac{c_1}{c_0}\exp\left[-\left(\sqrt{2\pi a}-\sqrt{2a\ln(4\pi a/\sigma_{tot})}\right)p\theta\right]\cos\left(\sqrt{2\pi a}\,p\theta-\varphi\right).$$

The authors note good agreement of the calculations performed according to this equation with the experimental results given in [36] at energies of 9.2, 10.1, 11.1, and 12.1 GeV. However, it is more difficult to match the calculations with more exact data from [37] in which detailed measurements were carried out in the range $|t| \sim 1$ (GeV/c)^2. A description of the results of [37] is given in the paper by the author [45] on the basis of the generalized equation (18).

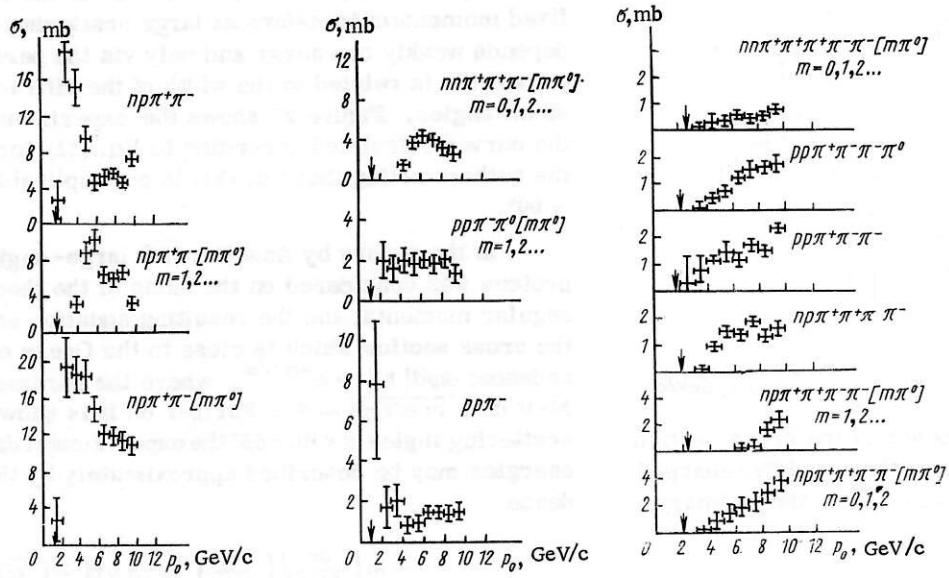

Fig. 34. Dependence of the cross sections of the partial reaction in np collisions on the primary momentum.

It is assumed that scattering occurs in three discrete interaction regions (i.e., quantization of the impact parameters or of the mean-square momenta occurs):

$$\langle p_\perp^2\rangle_1^{1/2}:\langle p_\perp^2\rangle_2^{1/2}:\langle p_\perp^2\rangle_3^{1/2}=1:2:3. \tag{23}$$

Further, summation of the partial amplitudes corresponding to the values $\langle p_\perp^2\rangle_i^{1/2}$ is assumed with allowance for the relative phase shift φ_i. On the basis of this the following equation is obtained for the differential cross sections:

$$\frac{d\sigma}{d(-t)}=\left[c_1\exp\left(-\frac{p_\perp^2}{\langle p_\perp^2\rangle}\right)+c_2\exp\left(-\frac{p_\perp^2}{4\langle p_\perp^2\rangle}\right)+c_3\exp\left(-\frac{p_\perp^2}{9\langle p_\perp^2\rangle}\right)\right.$$
$$+2(c_1c_2)^{1/2}\cos\varphi_2\exp\left(-\frac{p_\perp^2}{\frac{8}{5}\langle p_\perp^2\rangle}\right)+2(c_1c_3)^{1/2}\cos\varphi_3\exp\left(-\frac{p_\perp^2}{\frac{9}{5}\langle p_\perp^2\rangle}\right)$$
$$\left.+2(c_2c_3)^{1/2}\cos(\varphi_2-\varphi_3)\exp\left(-\frac{p_\perp^2}{\frac{72}{13}\langle p_\perp^2\rangle}\right)\right]\left(1+\frac{t}{2p_c^2}\right). \tag{24}$$

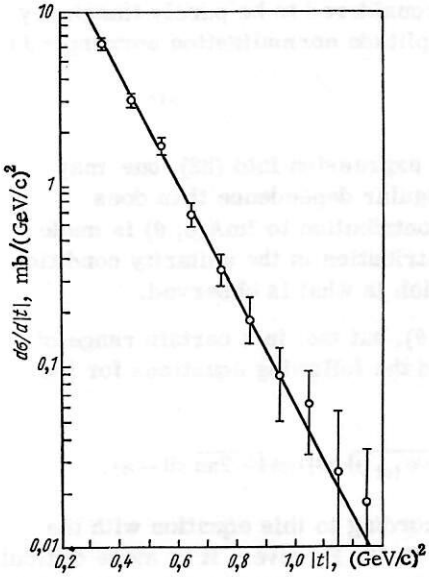

Fig. 35. Differential cross sections for elastic np scattering for 8 < E_{kin} < 10 GeV.

Figure 28 displays the experimental data for scattering at 19.2 GeV/c from [37] and the curve calculated according to Eq. (24) when the parameters were assumed equal to $\langle p_\perp^2\rangle^{1/2}=0.35$ GeV/c; c_1, c_2, c_3 in units 10^{-27} cm^2/(GeV/c)^2 were equal to 88, 0.15, 0.001; $\varphi_2=150°$, $\varphi_3=0°$. Equation (24) describes well-known experimental data for other values of high energy as well, the principal parameter $\langle p_\perp^2\rangle^{1/2}$ being constant within the limits of the accuracy with which they can be determined from the experimental errors: $\langle p_\perp^2\rangle^{1/2}=0.35\pm0.01$ GeV/c. The central point in the model proposed is, however, not the constancy of the parameter $\langle p_\perp^2\rangle$, which may be dynamically variable as a function of energy, but the condition (23).

If in Eq. (23) we do not restrict the analysis to three values and introduce $\langle p_\perp^2\rangle$, c_1, c_2, c_3, then for $d\sigma/d(-t)$ we have the following equation instead of (24):

$$\frac{d\sigma}{d(-t)}=\left\{\sum_{k=1}^{n}c_k\exp\left(-\frac{p_\perp^2}{k^2\langle p_\perp^2\rangle}\right)+2\sum_{k=2}^{n}(c_1c_k)^{1/2}\cos\varphi_k\exp\left[-\frac{p_\perp^2}{2\langle p_\perp^2\rangle}\left(1+\frac{1}{k^2}\right)\right]\right.$$
$$\left.+2\sum_{\substack{k=2\\m=1}}^{k+m=n}(c_kc_{k+m})^{1/2}\cos(\varphi_k-\varphi_{k+m})\exp\left[-\frac{p_\perp^2}{2\langle p_\perp^2\rangle}\left(\frac{1}{k^2}+\frac{1}{(k+m)^2}\right)\right]\right\}\left(1+\frac{t}{2p_c^2}\right). \tag{25}$$

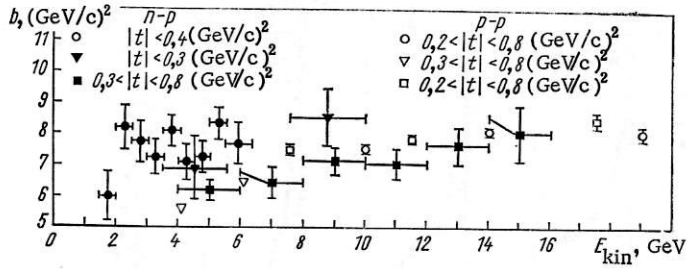

Fig. 36. Dependence of the slope parameter b of elastic np and pp scattering on E_{kin} of the primary nucleon.

From the values of c_1, c_2, c_3 given earlier it follows that the convergence of the sums in (25) is rapid. Equations (24) and (25) yield $d\sigma/d(-t) \to 0$ for a scattering angle $\theta \to 90°$. Consequently, it is necessary to introduce a small additional term which is essential for $\theta \to 90°$ and makes practically no contribution to the total cross section. Integrating Eq. (24), we obtain the total elastic scattering cross section:

$$\sigma_{ela} = \left[c_1 + 4c_2 + 9c_3 + \frac{16}{5}(c_1c_2)^{1/2}\cos\varphi_2 + \frac{18}{5}(c_1c_2)^{1/2}\cos\varphi_3 + \frac{144}{13}(c_2c_3)^{1/2}\cos(\varphi_2 - \varphi_3)\right]\langle p_\perp^2\rangle. \quad (26)$$

The values of σ_{ela} determined from Eqs. (26) for chosen values of $-\langle p_\perp^2\rangle$, c_1, c_2, c_3 are in agreement with experimental data which for the time being, regrettably, are known with an error of at least 10%.

2.3. Scattering in the Range of Angles near 90°

An experimental peculiarity of scattering events at small angles when the energy is fixed lies in the fact that the differential cross section tends to a constant value for $\theta \to 90°$. With increasing energy, and likewise for fixed $|t|$ an abrupt decrease of the cross sections near the limiting values occurs (see Fig. 29). An explanation of these phenomena is advanced on the basis of opposite models. In the first model scattering at $\theta \to 90°$ is caused by the processes which occur at smaller angles. In the second model, which is based on statistical theory, the formation of an excited system occurs and in a particular case its decay into two primary particles. It is evident that this process must yield an isotropic angular distribution in the center of mass system and consequently also a contribution to the differential cross sections at all angles. In [46] the central collisions are assumed to be those for which thermal equilibrium is established; i.e., the collision time is sufficient for the propagation of a shock wave forward and back in the portion of nucleon which does not intersect another. By determining the probability of central collisions and the statistical weight of the elastic channel for the decay of an excited system, Hagedorn obtained the following equation for the differential elastic-scattering cross section:

$$\frac{d\sigma}{d\Omega} = \frac{\sigma_{in}}{2\pi}\cdot\frac{4m^2}{s}\exp\left[-3.25\left(\sqrt{s}-2\right)\right], \quad (27)$$

where σ_{in} is the total cross section for inelastic scattering, a $\sqrt{s}$ is taken in nucleon-mass units. This equation ensures the abrupt decrease of the cross section with increasing energy and shows agreement with experiments.

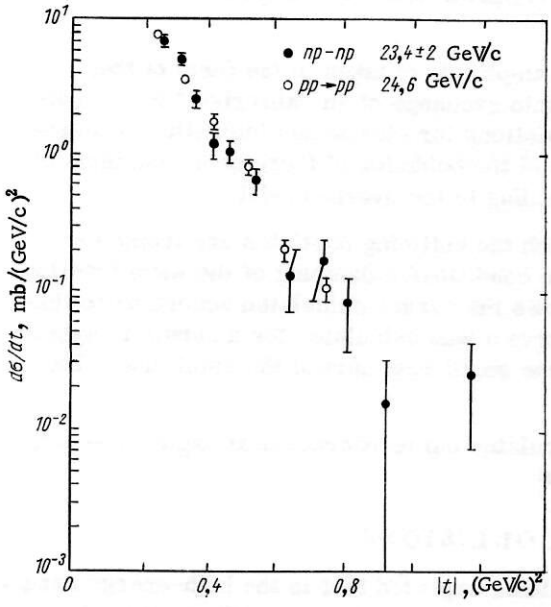

Fig. 37. Differential cross sections for elastic pp and np scattering in the momentum range ~ 21-25 GeV/c.

It is of interest to carry out an analogous calculation according to the P. Rotelly model [1] expounded in Sec. 1.1, which was in accord with experimental data on the dependence of the number of produced particles on energy and likewise on the ratio $K^{\pm}/\pi^{+}$; consequently, one can calculate the probability of elastic nondiffractional scattering. In [47–49] scattering at high energies is considered as a random process by means of which the angular distribution of the elastic scattering is also explained. In these papers the conditions were obtained

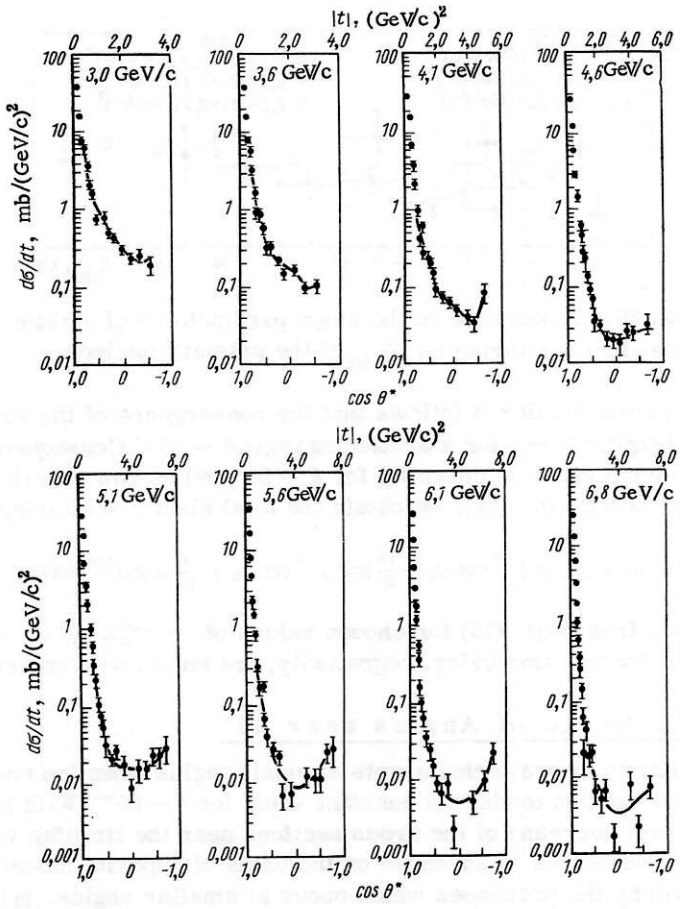

Fig. 38. Dependence of the differential cross section for elastic np scattering on cos θ^*.

for the correlation of the longitudinal and transverse components of the momentum, and likewise for the dispersions; on the basis of this it was concluded that a sudden "emergence onto a plateau" is possible for the elastic-scattering differential cross sections at transverse momenta which are comparable with the energy of the scattering particles.

In the hybrid model developed by Chiu [50] the scattering amplitude is taken in the form of the sum of the optical diffraction part and the part which develops into exchange of an "absorbed" Regge pole. This model predicts, in particular, that the differential cross sections for elastic and inelastic processes must have an identical dependence on t at large $|t|$ regardless of the behavior of these cross sections at small $|t|$. Figure 30 shows the result of the calculations according to the hybrid model.

In the papers by Yang [51, 52] a model is proposed in which the colliding particles are treated as finite extended objects which penetrate each other. Under these conditions a damping of the wave function occurs, the result of which is elastic scattering. Figure 31 shows the curves calculated according to this model using the dipole electromagnetic proton form factor. Curve a was calculated for a purely imaginary scattering amplitude; curve b was calculated with inclusion of the small real part of the amplitude. The dashed lines illustrate the experimental results.

It follows from Fig. 31, that although the slope of the calculated curve decreases at angles $\theta \to 90°$, they nevertheless yield a more rapid fall-off of the cross section.

III. NEUTRON – PROTON COLLISIONS

From general propositions on strong interactions it should be expected that in the high-energy range, neutron-proton interactions have properties similar to proton interactions. These reactions allow the

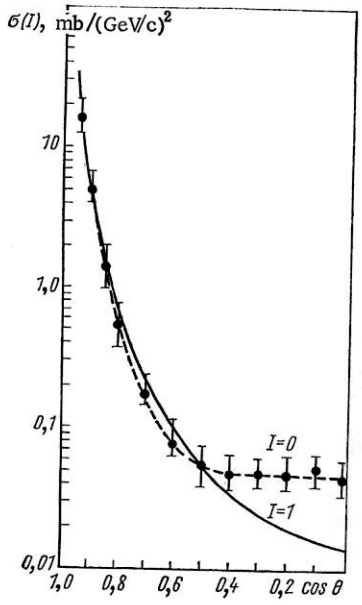

Fig. 39. Dependence of the differential cross section for elastic np scattering at 5 GeV/c for states with isotopic spin 0 and 1 on cos θ.

details of the interaction to be revealed from the asymmetry of the colliding particles in the center of mass system and information on the role of identity to be given for purposes of theory. In np collisions an additional process – elastic charge exchange – occurs also.

Data on neutron-proton interactions are less detailed and exact as a consequence of the fact that experimentally the study of np collisions present substantially greater difficulties – there are no primary intense monochromatic neutron beams and no pure neutron targets. In investigating np collisions the simplest way is to perform experiments in proton beams using nuclear targets (deuterium targets are the best version in electron experiments) and likewise experiments in filling bubble chambers with deuterium. However, the nuclear binding of a neutron complicates an analysis of the experiment. The second way is to perform experiments using hydrogen targets in neutron beams which are obtained as a result of the interaction of primary particles. In experiments on elastic np scattering the detection of a scattered neutron and a recoil proton allows the kinematic relationships to be used for determining the energy of the primary neutron.

3.1. The Total Cross Sections

Figure 32 shows the energy dependence of the total cross sections for np- pp-collisions. As is evident in the figure, it should be assumed that at the energy which is the largest of those achieved the cross sections are identical within the limits of the experimental errors. This is in agreement with the papers by I. Ya. Pomeranchuk and L. B. Okun' [53, 54] on the equality of the asymptotic limit of the total cross sections for interaction of particles belonging to one multiplet with a stipulated target.

3.2. Production of Particles and Resonances

The energy dependence of the average number of particles produced in np collisions is close to the analogous dependence for pp collisions, but the lower accuracy of the experiments and the narrower energy range in which they are conducted for the time being does not allow the exponents to be estimated in the equation $n(E) = E^x$.

In a number of papers data have been obtained on the energy dependence of the partial cross sections and effective masses in np reactions. The results of investigations carried out in papers by V. I. Moroz [55, 56, 57] involving the irradiation of a propane bubble chamber with neutrons are shown in Fig. 33. This figure presents the dependence of the production cross sections of events having three or five charged particles, as well as the ratio of these cross sections, as a function of momentum.

Figure 34 presents the cross sections of various reactions as a function of energy.

In these experiments effective-mass distribution were obtained for the systems: $p\pi^+\pi^+$, $p\pi^-\pi^-$ and $p\pi^+\pi^-$ which were formed in the following reactions, respectively:

$$np \to \begin{cases} n\Delta^{++}\pi^+\pi^-\pi^- (m\pi^0) \\ p\Delta^-\pi^+\pi^+\pi^- (m\pi^0) \\ \Delta^{++}\Delta^-\pi^+\pi^- (m\pi^0). \end{cases}$$

These distributions, according to the conclusions of the authors of [57], can be explained if the mass of the isobars Δ^{++} and Δ^- is equal to 1236 MeV, while in the mass range 1400 to 1700 MeV, the upper boundaries for the formation of the Δ^{+++} isobars having isotopic spin 5/2 and decaying into $p\pi^+\pi^+$ amounts to ~ 30 μb.

In the experiments by B. A. Shakhbazian [58] which were likewise carried out by irradiating a propane bubble chamber with neutrons having an average momentum of 7.5 GeV/c, resonance phenomena in two-baryon systems were discovered for the first time. It was determined that near the sum of the masses

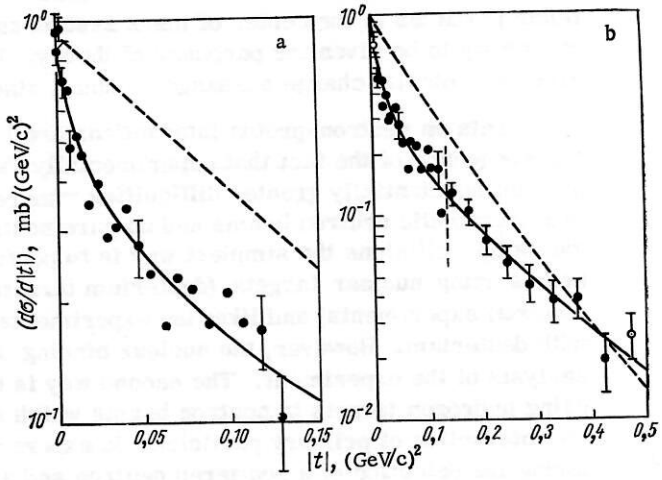

Fig. 40. Dependence of the differential cross section for elastic np-charge exchange on $|t|$ at $\theta_{lab} = 0$ to 45 mrad (a) and 0 to 90 mrad (b).

λ, p the spectrum may be explained by resonance at the virtual level of the λp system having an energy Q = (4.4 ± 0.1) MeV. This result has been substantiated in pp and KD collisions in [59] and [60].

3.3. Elastic Scattering

In the range of small scattering angles the differential cross sections $d\sigma/d(-t)$ of elastic np and pp scattering have an identical slope for equal primary energies, and the diffraction peaks are compressed with increasing energy. In the 3 to 7 GeV range this is shown, for example, by the results of [61] where $d\sigma/d(-t) \sim A \exp(bt)$ was obtained for $|t| \leq 0.4$ (GeV/c)^2. On the basis of this the authors of [61] express support of the idea that the distributions of hadron matter in a neutron and photon are very similar.

In [62] the differential cross sections were determined for neutrons in the kinetic energy range 8 to 10 GeV. They are shown in Fig. 35, where for t = 0 they are normalized to the value of the cross section based on the optical theory, and the straight line in the figure corresponds to $\sim \exp(A + bt)$.

The aggregate results of experiments performed by many groups of authors in the region of the diffraction peaks are displayed in Fig. 36. It follows from this figure that in the energy range from 10 to 20 GeV the parameter b is close to 8 (GeV/c)$^{-2}$; i.e., it is identical to its average value in the case of pp scattering according to Table 1. This indicates coincidence of the effective interaction radii in elastic pp and np collisions. Note likewise that the value b = 8 (GeV/c)$^{-2}$ is close to $1/\langle p_\perp^2 \rangle = 8.1$ (GeV/c)$^{-2}$ from Eqs. (7), (18) for the value $\langle p_\perp^2 \rangle^{1/2} \equiv 0.35$ GeV/c which was used.

For larger scattering angles, including ~ 90°, it is not clear a priori what the behavior of the np-scattering cross section is in comparison with the pp-scattering cross section. In [38], for example, the notion was stated that for 90° at high energies the cross section of elastic np scattering may amount to ~ 1/2 elastic pp-scattering cross sections. The difficulty in predicting the behavior of the cross sections at large scattering angles, as noted in [61], is associated with the absence of a simple model and a large number of independent scattering amplitudes. For each isotopic spin state J = 1 and J = 0 there are five independent scattering amplitudes, each having its own symmetry property near 90° in accordance with the generalized Pauli principle.

Figure 37 displays the cross sections of np and pp scatterings in the $|t| = 0.2$ to 1.2 (GeV/c)^2 range according to the data of [63, 64] for energies ~ 24–25 GeV. As is evident from the figure, the cross sections have closely similar values.

In [6] it was found that in the 4 to 7 GeV range the ratio between the cross sections is

$$\frac{d\sigma}{d(-t)}(np) \Big/ \frac{d\sigma}{d(-t)}(pp) = 1.1 \pm 0.1.$$

Thus, it should be concluded that closeness of the cross sections for elastic np and pp scattering holds throughout the entire range of angles. Note, however, that as yet no details or precise data exist for np scattering for $|t| \sim 1$ (GeV/c)^2 where a fine structure of the cross sections of elastic pp scattering was manifested.

Let us dwell on the dependences of the cross sections on the isotopic spin. Figure 38 from [65] shows the differential cross sections of elastic np scattering in the energy range from 3 to 6.8 GeV, including scattering angles θ larger than 90° in the center of mass system. According to the figure, symmetry of the cross sections as a function of θ is observed when $|\cos\theta| \leq 0.3$. This symmetry indicates the smallness of the interference term for the scattering amplitudes in states having isotopic spins 1 and 0.

Figure 39 from [61] shows the dependence of the cross sections σ^1 of elastic np scattering in the isotopic spin state J = 1 at an energy of 5 GeV on $\cos\theta$ (σ^1 are identical with the cross sections of pp scattering), as well as the same dependence of the cross sections σ^0 for J = 0. It follows from the figure that σ^0 is three times as large as σ^1.

3.4. Elastic Charge Exchange

Elastic charge exchange is one of the cases of exchange scattering (i.e., a process in which the particles exchange quantum numbers). In the case of np collisions an exchange of electric charge occurs. The charge exchange, on the other hand, may be treated as a case of elastic scattering, since the initial and final particles are identical, while on the other hand it may be treated as an inelastic process for an individual particle.

Experiments at various energies showed that np-charge exchange has, similarly to elastic scattering, a sharp diffraction peak. This is evident, for example, in Fig. 40 of [66] at 8 GeV/c. The dashed lines in the figure are processed data on elastic np scattering at 8.9 GeV/c from [33]. The abrupt growth of the differential cross section for charge exchange can be understood by starting from the fact that the transfer of charge between a neutron and a proton is associated with a small energy transfer. In [67] the authors explain exchange and elastic scattering as coherent excitation of particles during passage through an absorptive medium.

CONCLUSION

In aggregate, the results of the experiment which have been considered show that their explanation cannot be achieved using any of the existing models of nucleon-nucleon interaction. Each of the models is better fitted to explain specific phenomena, and even in this case the substantiation or invalidation of the model is limited by the low experimental accuracy (for example, the total cross sections for elastic pp scattering are known with an error of at least 10%). A substantial improvement of the known experimental data is required, as well as a discovery of new regularities. In this respect the results of experiments carried out on the Serpukhov accelerator, as well as on the colliding-beam accelerator at CERN, will have great significance. In the latter experiments an extensive program of research on elastic and inelastic pp collisions has been planned for a high energy equivalent in the laboratory system (1650 GeV).

However, obtaining precision data in the energy range ~ 10 GeV is also no less important.

LITERATURE CITED

1. P. Rotelly, Phys. Rev., 182, 1622 (1969).
2. R. Hagedorn, TH-1027 CERN (1969).
3. M. Firebugh, et al., Bull. Amer. Phys. Soc., 11, 360 (1966).
4. S Holmgren, et al., Nuovo Cimento, 51, 305 (1967).
5. J. Bartke, et al., Nuovo Cimento, 29, 8 (1963).
6. A. Erwin, Nucl. Phys., B17, 445 (1970).
7. E. Lillethun, Proceedings of the Lund International Conference on Elementary Particles, Stockholm (1969), p. 167.
8. E. V. Anderson, et al., Phys. Rev. Lett., 16, 855 (1966).
9. L. Bertocchi and E. Ferrari, High-Energy Physics, Pergamon Press (1967), p. 71.
10. J. C. Rushbrooke, et al., Fourteenth International Conference on High-Energy Physics, Vienna (1968), p. 161.

11. R. Hagedorn, Nuovo Cimento, Suppl., 6, 311 (1968).
12. E. V. Anderson, et al., Phys. Rev. Lett., 19, 198 (1967).
13. K. D. Tolstov, Preprint of the Joint Institute for Nuclear Research R1469 [in Russian], Dubna (1963).
14. B. P. Bannik, et al., Yadernaya Fizika, 9, 590 (1959).
15. D. Dekkers, et al., Phys. Rev., 137B, 962 (1965).
16. A. D. Krisch, Symposium on Multiparticle Production, ANL/HEP 6909 (1968).
17. W. Heisenberg, Physical Principles of Quantum Theory [Russian translation] (1962).
18. S. G. Asbury, Bull. Amer. Phys. Soc., 14, No. 29, A61 (1969).
19. S. Turkot, Topical Conference on High-Energy Collisions of Hadrons, CERN (1968) p. 316.
20. E. V. Anderson and C. B. Collins, Phys. Rev. Lett., 19, 201 (1967).
21. H. A. Kastrup, Phys. Rev., 147, 1190 (1966); N. W. Lewis, et al., Phys. Rev., 79, 127 (1948).
22. J. V. Day, A. D. Krisch, et al., Phys. Rev. Lett., 23, 1469 (1969).
23. Chan Hong Mo, TH-1089, CERN (1969).
24. H. Satz, Nucl. Phys., B14, 366 (1969).
25. P. K. Markov, et al., Zh. Éksperim. i Teor. Fiz., 38, 1471 (1960).
26. B. A. Carrigan, et al., Phys. Rev. Lett., 24, 689 (1970).
27. D. Harting, Nuovo Cimento, 38, 60 (1965).
28. K. J. Foley, R. S. Jones, and S. J. Lindenbaum, Phys. Rev. Lett., 19, 857 (1967).
29. G. G. Beznogikh, et al., Yadernaya Fizika, 10, 1212 (1969).
30. K. A. Ter-Martirosyan, Preprint of the Institute of Theoretical and Experimental Physics 417 [in Russian], Serpukhov (1964).
31. K. D. Tolsov, Izv. Akad. Nauk SSSR, Ser. Fiz., 31, 1480 (1967); Yadernaya Fizika, 1, 832(1965).
32. L. F. Kirillova, et al., Yadernaya Fizika, 1, 533 (1965).
33. K. Foley, et al., Phys. Rev. Lett., 11, 425 (1963).
34. C. W. Akerlof, et al., Phys. Rev. Lett., 17, 1105 (1966).
35. M. C. Ankenbrandt, et al., UCRL-17257, Berkeley (1966).
36. J. V. Allaby, F. Binon, and A. N. Diddens, Phys. Lett., 25B, 156 (1967).
37. J. V. Allaby, F. Binon, and A. N. Diddens, Phys. Lett., 26B, 67 (1968).
38. T. T. Wu. and C. N. Yang, Phys. Rev., 137B, 708 (1965).
39. T. Kinoshita, Phys. Rev. Lett., 12, 257 (1964).
40. A. Martin, Nuovo Cimento, 37, 671 (1965).
41. V. R. Garsevanishvili et al., Preprint of the Joint Institute for Nuclear Research, E2-4241, Dubna (1969).
42. A. A. Logunov and A. N. Tavkhelidze, Nuovo Cimento, 29, 380 (1963); A. N. Tavkhelidze, Lectures on the Quasipotential Method in Field Theory, Tata Institute, Bombay (1965).
43. A. A. Ansel'm and I. T. Dyatlov, Yadernaya Fizika, 6, 591 (1967); 6, 603 (1967).
44. I. V. Andreev and I. M. Dremin, Yadernaya Fizika, 8, 814 (1968).
45. K. D. Tolstov, Preprint of the Joint Institute for Nuclear Research D1-4001 [in Russian], Dubna (1968); Preprint of the Joint Institute for Nuclear Research R1-4666, Dubna (1969).
46. R. Hagedorn, Nuovo Cimento, 35, 216 (1965).
47. A. A. Logunov and O. A. Khrustalev, Preprint of the Institute of High-Energy Physics 67-64-K [in Russian], Serpukhov (1967).
48. A. A. Logunov and O. A. Khrustalev, Preprint of the Institute of High-Energy Physics STF-69-20 [in Russian], Serpukhov (1969).
49. A. A. Logunov and O. A. Khrustalev, Preprint STF-69-21 (1969).
50. C. B. Chiu and J. Finkelstein, Nuovo Cimento, 59A, 92 (1969).
51. T. T. Chou and C. N. Yang, Phys. Rev., 170, 1591(1968).
52. T. T. Chou and C. N. Yang, Phys. Rev., 175, 1832 (1968).
53. I. Ya. Pomeranchuk, Zh. Éksperim. i Teor. Fiz., 30, 429 (1956).
54. L. B. Okun' and I. Ya. Pomeranchuk, Zh. Éksperim. i Teor. Fiz., 30, 424 (1956).
55. V. I. Moroz, A. V. Nikitin, and Yu. A. Troyan, Yadernaya Fizika, 9, 792 (1969).
56. V. I. Moroz, A. V. Nikitin, and Yu. A. Troyan, Yadernaya Fizika, 9, 374 (1969).
57. V. I. Moroz, A. V. Nikitin, and Yu. A. Troyan, Yadernaya Fizika, 9, 565 (1969).
58. V. F. Vishnevskii, V. I. Moroz, and B.A. Shakhbazyan, Pis'ma Zh. Éksperim. i Teor Fiz., 5, 307 (1967).
59. J. T. Read, Phys. Rev., 168, 1495 (1968).

60. T. H. Tan, Phys. Rev. Lett., 23, 395 (1969).
61. J. Cox and M. L. Perl, Phys. Rev. Lett., 21, 645 (1968).
62. J. Emgler, et al., Phys. Lett., 29B, 321 (1969).
63. G. Bellettrini, Fourteenth International Conference on High-Energy Physics, Vienna (1968).
64. C. W. Akerlof, et al., Phys. Rev., 159, 1138 (1967).
65. J. Cox and L. Perl, Phys. Rev. Lett., 21, 641 (1968).
66. G. Manning, et al., Nuovo Cimento, 41A, 167 (1966).
67. N. Byers and C. N. Yang, Phys. Rev., 142, 976 (1966).